Pergamon

Geochimica et Cosmochimica Acta, Vol. 67, No. 12, pp. 2269–2288, 2003

0016-7037/03 $30.00 + .00

doi:10.1016/S0016-7037(00)01403-5

Mineralogy of silicate inclusions of the Colomera IIE iron and crystallization of Cr-diopside and alkali feldspar from a partial melt

HIROSHI TAKEDA,[1,2,*] WEIBIAO HSU,[3] and GARY R. HUSS[2,‡]

[1]Research Institute, Chiba Institute of Technology, 2-17-1 Tsudanuma, Narashino City, Chiba 275-0016, Japan
[2]Division of Geological and Planetary Science, California Institute of Technology, Pasadena, CA 91125, USA
[3]Purple Mountain Observatory, 2 West Beijing Road, Nanjing 210008, China

(*Received November* 7, 2001; *accepted in revised form December* 2, 2002)

Abstract—We studied the mineralogy, mineral chemistry, and compositions of 48 interior silicate inclusions and a large K-rich surface inclusion from the Colomera IIE iron meteorite. Common minerals in the interior silicate inclusions are Cr diopside and Na plagioclase (albite). They are often enclosed by or coexist with albitic glasses with excess silica and minor Fe-Mg components. This mineral assemblage is similar to the "andesitic" material found in the Caddo County IAB iron meteorite for which a partial melt origin has been proposed. The fairly uniform compositions of Cr diopside ($Ca_{44}Mg_{46}Fe_{10}$) and Na plagioclase ($Or_{2.5}Ab_{90.0}An_{7.5}$ to $Or_{3.5}Ab_{96.1}An_{0.4}$) in Colomera interior inclusions and the angular boundaries between minerals and metal suggest that diopside and plagioclase partially crystallized under near-equilibrium conditions from a common melt before emplacement into molten metal. The melt–crystal assemblage has been called "crystal mush." The bulk compositions of the individual composite inclusions form an array between the most diopside-rich inclusion and plagioclase. This is consistent only with a simple mechanical mixing relationship, not a magmatic evolution series. We propose a model in which partly molten metal and crystal mush were mixed together by impact on the IIE parent body. Other models involving impact melting of the chondritic source material followed by growth of diopside and plagioclase do not easily explain near equilibrium growth of diopside and Na plagioclase, followed by rapid cooling. In the K-rich surface inclusion, K feldspar, orthopyroxene, and olivine were found together with diopside for the first time. K feldspar (sanidine, $Or_{92.7}Ab_{7.2}An_{0.1}$ to $Or_{87.3}Ab_{11.0}An_{1.7}$) occurs in an irregular veinlike region in contact with large orthopyroxene crystals of nearly uniform composition ($Ca_{1.3}Mg_{80.5}Fe_{17.8}$ to $Ca_{3.1}Mg_{78.1}Fe_{18.9}$) and intruding into a relict olivine with deformed-oval shape. Silica and subrounded Cr diopside are present within such K-feldspar regions. Some enrichments of the albite component have been detected at the end of curved elongated nodules of K feldspar intruded into the mafic silicates. The textural relationships suggest that a K-rich melt was present. A K-rich melt is neither the first melt of a chondritic system nor a differentiation product of a Na-rich partial melt of chondritic material. The K-rich material may have originated as a fluid phase that leached K from surrounding materials and segregated by a mechanism similar to that proposed for the Na-rich inclusions. *Copyright © 2003 Elsevier Science Ltd*

1. INTRODUCTION

Alkali-rich silicate inclusions in the IIE irons were the first constituents in iron meteorites for which reliable ages were obtained (Wasserburg et al., 1968; Sanz et al., 1970). During one such investigation, K-feldspar pheonocrysts were found in the surface of Colomera (Wasserburg et al., 1968). Although much work has been performed on Colomera over the years (Prinz et al., 1983; Armstrong et al., 1990; McCoy, 1995), comprehensive mineralogical studies have not been reported. Silicate inclusions in eight known IIE irons show diversity in mineralogy (e.g., Bunch et al., 1970; Wasson et al., 1989; Casanova et al., 1995; McCoy, 1995; Ikeda and Prinz, 1996; Ruzicka et al., 1999), and Colomera, Kodaikanal (Bence and Burnett, 1969) and Elga (Osadchii et al., 1981) contain alkali-rich, highly differentiated silicate inclusions. Ikeda and Prinz (1996) and Ikeda et al. (1997a) also noted the presence of such silicate inclusions in the IIE iron, Miles. To elucidate the formation mechanism of alkali-rich materials, we carried out a mineralogical study of 48 silicate inclusions found in four new polished slices of Colomera and of a new polished thin section (PTS) made from a large chip of the surface inclusion studied by Wasserburg et al. (1968). Some rare earth element (REE) data has been reported for some of the Colomera inclusions described here (Hsu et al., 1997). In this article, we report representative REE data to support our mineralogical interpretation.

Because of the diversity of silicate inclusion types in IIE irons, a range of models has been proposed for their origin. Bogard et al. (2000) showed evidence of a complex parent body evolution for IIE irons on the basis of ^{39}Ar-^{40}Ar ages. The origin of essentially chondritic inclusions is simpler than that of the evolved types. Bild and Wasson (1977) noted that Netschaëvo includes recrystallized chondrules typical of those found in type 6 ordinary chondrites. A common theme in formation models is impact-generated melting and mixing (e.g., Olsen et al., 1994). Ruzicka et al. (1999) suggested two possible models for forming IIE iron meteorites, both involving collision between an FeNi-metal projectile and a silicate-rich target of H-chondrite affinity. Wasserburg et al. (1968) pro-

* Author to whom correspondence should be addressed (takeda@pf.it-chiba.ac.jp).
‡ *Present address:* Department of Geological Sciences and Center for Meteorite Studies, Arizona State University, Tempe, AZ 85287-1404, USA.

posed that the silicates (plums) formed from strongly differentiated silicate melts trapped in the cooling metal (pudding) after a shock event. Ikeda et al. (1997a) proposed that silicate inclusions in Miles are the crystallization products of silicate melts that were produced by equilibrium or impact partial melting of an H chondritic precursor, and that the degree of melting was variable. However, the formation mechanism of alkali-rich melts has not been clearly understood.

Observations from IAB irons may hold the key to understanding the origin of the alkali-rich materials in IIE irons. Plagioclase-rich materials are present in silicate inclusions in the IAB irons, Y791058 and Caddo County, and lodranite/acapulcoite, EET84302 (Takeda et al., 1993, 1994, 2000; Stewart et al., 1996; Yugami et al., 1998). Magnesium-rich silicates in lodranites/acapulcoites and winonaites/IAB irons have been identified as residues of partial melting (Takeda et al., 1994, 2000; McCoy et al., 1997), but basalts representing their solidified partial melts have not been found in the meteorite collections or asteroids. By applying large-area (up to 7 cm in length) chemical mapping techniques with microfocus XRF analysis equipment, Takeda et al. (1994, 2000) found plagioclase-augite(diopside)-rich (andesitic) regions in a large slab of Caddo County. The Na-Al-Ca-rich andesitic regions have been considered to be candidates for partial melts of chondritic materials. The difference between such partial melts and eucritic materials have been discussed partly in connection with the origin of the HED meteorites (Takeda, 1997). The finding of Na-Al-Ca-rich materials of the IAB irons promoted renewed interest in the alkali-rich inclusions in Colomera. The mineralogical assemblages and their textural relationships are useful in interpreting the formation mechanism of the Colomera inclusions. The results were compared with alkali-feldspar-rich clasts found of other IIE and IAB irons (Takeda et al., 2000) to deduce their common formation mechanisms.

2. EXPERIMENTAL METHODS

Four new polished slices, approximately 1.7 × 2.0 cm across and 5 mm thick, were cut from two slices CF1A and CF1F preserved at the Lunatic Asylum, Caltech. They are remainders of slice CF1 cut previously from the slab II (Caltech cuts), which was cut from the main mass of the meteorite (see Fig. 1 of Sanz et al., 1970). The slices were each embedded in plastic discs and one side was polished. A new polished thin section PTS, Cl LF, was prepared from a large fragment (LF) that was separated previously from a surface inclusion rich in K feldspar (Wasserburg et al., 1968). Four other polished thin sections previously made at Caltech were also studied for comparison (IIABD1, L1, J1, IIB-GFA). Many polished grain mounts (e.g., C1-3, C5-1, C7) made from silicate inclusions of Colomera by Sanz et al. (1970) were investigated under an optical microscope.

Textural relationships in polished sections were investigated by scanning electron microscopy. The scanning electron microscope used was a JEOL 840 with an energy-dispersive spectrometer. Modal mineral abundances for the silicate inclusions were obtained via a method similar to that used in the Chemical Map Analysis technique of Yugami et al. (1998) by processing the maps with the Adobe Photoshop program. Elemental distribution maps of PTS C1 LF and section CF1F1 were obtained with the JEOL 8800 electron microprobe at Chiba Institute of Technology and on a JEOL 8900 electron probe microanalyzer (EPMA) at Ocean Research Institute of the University of Tokyo. Reflected light photographs were converted into mineral distribution maps with the Adobe Streamline program by combining them with the back-scattered electron images. Abundances of major minerals in Colomera were obtained by measuring areas of a particular mineral on the mineral distribution maps.

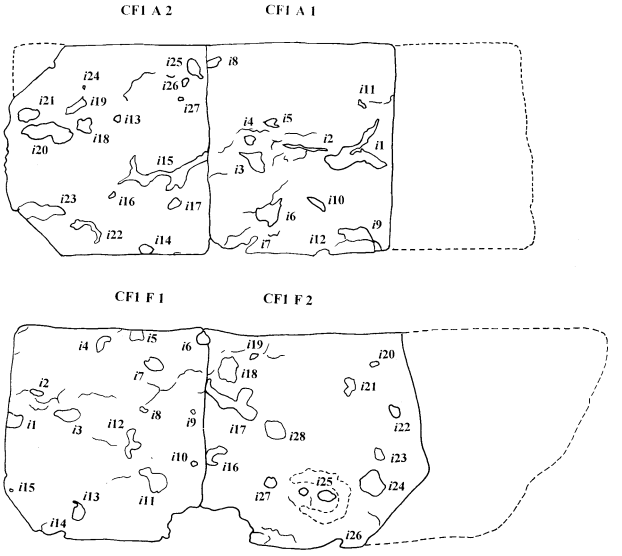

Fig. 1. Locations and shapes of silicate inclusions in Colomera CF1A and CF1F. Inclusion numbers are assigned to the inclusions.

Chemical compositions of minerals were measured with a JEOL JCXA-733 EPMA at Caltech. Acceleration voltage was 15 kV and beam current was 15 nA on a Faraday cage and the beam was rastered over 5 × 5 μm. X-ray intensities were corrected by the ZAF method. Rhyolite glass from Yellowstone (VG-568) from the Smithsonian Institution was used as a standard for glass analyses. Counting time for minerals was 45 s, but 15 s was used for glass analyses to avoid alkali loss. Chemical compositions of minerals in the C1LF PTS and the CF1F1 section were obtained with the same type of EPMA at Ocean Research Institute of Unviersity of Tokyo. The EPMA data are deposited at Planetary Materials Database of Mineralogical Institute, University of Tokyo.

REE data for albite, diopside, orthopyroxene, Ca-phosphates, and glass were obtained with secondary ion mass spectrometry with PANURGE, a Cameca IMS 3f instrument at Caltech. Samples were bombarded with primary O^- ions with a beam current of 1 to 5 nA and an impact energy of 17 kV. The primary beam diameter on the samples was ~5 to 15 μm. The secondary ion mass spectrometer was operated at low mass resolving power and with a ~30 V energy window. Secondary ions were energy filtered with a sample offset of 100 V to suppress signals from complex molecular interferences and measured signals were deconvolved into REE and REE-oxide components following standard techniques (Zinner and Crozaz, 1986; Fahey et al., 1987). Absolute concentrations of each element were determined on the basis of empirical relationships between measured peak/$^{30}Si^+$ ratios, normalized to the SiO_2 content determined by prior EMPA analysis. Standards were a synthetic Ti-pyroxene glass, NBS-612 glass, plagioclase glass, and Durango apatite. Analytical precision is typically better than 10% at parts-per-million–level concentrations, and absolute abundance calibrations are accurate at the 10% level.

3. RESULTS

3.1. Interior Inclusions: Major Types, Mineralogy, and Relative Abundances

The 48 interior inclusions found and studied in four polished slices and four polished thin sections can be divided into four types: (1) Na-plagioclase inclusions (27%); (2) glassy inclusions with compositions similar to Na plagioclase but with excess silica and minor ferromagnesian components (38%); (3) composite inclusions consisting of more than two minerals such as Cr diopside, Na plagioclase, orthopyroxene, chromite,

Table 1. Mineral assemblages, shapes and sizes of silicate inclusions in Colomera.[a]

Section No.	Incl. No.	Size	Shape	Glass	Felds	Cr-Di	Opx	Chrom.	Tro.	Other
C1 LF	si	LL			(Sd)**	*	**			*
CF1A1	i1	L	Elongated, branched		****	**			<	
CF1A1	i3	M	Triangle		**	***			<	
CF1A1	i4	S	Round		**	***				
CF1A1	i5	S	Round	****	*					
CF1A1	i6	M	Triangle	<	****	*				
CF1A1	i10	M	Elongated	****						
CF1A2	i13	S	Round		****					
CF1A2	i15	L	Elongated, branched	*	*	**			<	
CF1A2	i16	S	Rectangle	****						
CF1A2	i17	S	Subround		****					
CF1A2	i18	M	Irregular		***	*		<		
CF1A2	i19	M	Elongated rectangle		****			<		
CF1A2	i20	L	Extended, S-shaped		***	**				
CF1A2	i21	M	Oval	****					<	*
CF1A2	i22	S	Elongated						****	
CF1A2	i23	M	Elongated		*	****				
CF1A2	i24	S	Subround, rectangle		****					
CF1A2	i25	M	Oval with tail		*	****				
CF1A2	i26	S	Round		****					
CF1A2	i27	S	Mit	***		**				<
CF1F1	i1	S	Subangular		****					
CF1F1	i2	S	Shoe-shape		****					
CF1F1	i3	M	Elongated oval		***					*
CF1F1	i4	S	Rounded L		****					
CF1F1	i5	M	Angular		****					
CF1F1	i6	S		****						
CF1F1	i7	M	13th day moon	****						
CF1F1	i8	S	Pointed rectangle	*	**	***			<	
CF1F1	i9	S	Round		***	***				
CF1F1	i10	S	Round		****					
CF1F1	i11	L	Penguin		****	*				
CF1F1	i12	M	Rounded W-shape	****		*				
CF1F1	i13	M	Oval with tail (fish)	***	*					*
CF1F2	i17	L	Subround Y-shape		***	**				
CF1F2	i19	M	Irregular rectangle		***	***				
CF1F2	i27	S	Maron		**					***
IIAB D1	i1	LL	Triple ball	***		**	<	<		
IIAB D1	i4	M	Subround quadrilateral	***	<			*	<	**
IIAB D1	i5	M	Subround quadrilateral	*			**			*
IIABGFA	i1	M	Elongated lense	****						
IIABJ1	i1	M	Elongated dunbell	***			**			
IIABJ1	i2	S	Quadrilateral	****						
IIABJ1	i3	M	Curved sward	****						
IIABJ1	i4	L	Rounded quadrilateral	***			*			*
IIABL1	i1	M	Circle	****				*		
IIABL1	i5	S	Tear drop	***			***			
IIABL1	i6	S	Irregular half circle	*			****			
IIABL1	i7	S	Elongated triple circle	****			*			

[a] LL = very large; L = large; S = small for size (Fig. 1). Numbers of * represent semiquantitative abundance. **** = major mineral. < = trace. Felds: Na-Feldspar, except for Sd (Sanidine). Chrom.: Chromite.

or Ca phosphate (25%); and (4) various ungrouped inclusions (10%). Distinguishing between glassy and feldspar-bearing inclusions is difficult, especially in the polished slices. The criteria used to identify glassy inclusion in polished slices were: (1) Si content larger than 3 for 8 oxygens, (2) Mg greater than 0.001 for 8 oxygens, and (3) total alkali content (K + Na + Ca) less than 1. According to this definition, some glassy inclusions have Na-plagioclase compositions. Plagioclase was identified by optical microscope whenever thin sections were available. Mineral assemblages and modal proportions of all inclusions studied in this work are summarized in Table 1. Locations of silicate inclusions in CF1A and CF1F are given in Figure 1 together with inclusion numbers used in Table 1.

Sodium-plagioclase inclusions, one of the most abundant types, are generally small and have rounded shapes. Some contain no other minerals, but others contain crystals of Cr diopside and a few contain Ca phosphate. CF1F i17 is one of the largest Na-plagioclase inclusions and has two branches (Fig. 1). One branch is mostly Na plagioclase with a hump of Cr diopside. CF1A i13 is a chestnut-shaped glassy inclusion with concave edge, where Na plagioclase has grown. Potassium feldspar was not identified in Na-plagioclase inclusions except in inclusion CF1F i3.

This is a slightly curved, elongated oval inclusion with mainly small silica and K feldspar, but its origin is not clear.

Glassy inclusions with compositions similar to Na plagioclase but with excess silica and minor ferromagnesian components are also abundant. They also tend to exhibit rounded shapes. Boundaries between metal and glass are always rounded. Some glassy inclusions contain Ca phosphate or small crystals of orthopyroxene. CF1F i12 has an octopus-like shape with a rounded glassy head and two legs of angular diopside crystals (Fig. 2a).

Composite inclusions typically consist of Na plagioclase, Cr diopside, and other minerals. Sodium plagioclase in these inclusions tends to have rounded shapes, whereas Cr diopside typically shows complex angular shapes. CF1A i19 consists mostly of Cr diopside and shows a rectangular shape. CF1A i1 and i15 are examples of large elongated, branched inclusions with rectangular shaped Cr-diopside crystals. CF1A i1 is one of the most complex-shaped inclusions and has a Y shape (Fig. 1). In one wing-shaped part and the central area, Cr-diopside crystals grew in albitic glass, and in the other two ends metal-Na-plagioclase boundaries are more rounded. CF1A i3 is a triangular inclusion with elongated neck of Cr diopside and CF1F i11 is a penguinlike inclusion with a body of angular Na plagioclase, two legs of Cr diopside and a head of mixtures of two minerals and tiny K-feldspar crystals (Fig. 2b). PTS IIABD1 il contains one of the largest Cr-diopside crystals found in our PTSs. This inclusion has a shape of triple composite spheres 0.93 mm long with sphere diameters of 0.46, 0.41, and 0.30 mm, respectively (Fig. 2c). CF1A i15 is another complex branched veinlike inclusion consisting mostly of Cr diopside with minor Na plagioclase (Fig. 3a). Inclusion boundaries with glass–metal contacts have rounded shapes, whereas those with mineral–metal contacts retain the angular shape of the silicate crystals. Such morphologic signatures indicate the crystals were present before emplacement in metal. Large elongated inclusions appear to show textures filling interstices of metallic grains. The presence of large irregular veinlike inclusion suggests that the metal was partly crystallized when the silicate melts and possibly crystals were incorporated. The metal–metal boundaries can be traced by veinlike schreibersite.

Several inclusions do not fit into the above categories. Inclusion CF1A i6 consists of Na plagioclase with minor granular inclusions of Cr diopside and a "tail" of chlorapatite. Inclusion CF1F i13 also has a tail of whitlockite attached to an usual inclusion of Na plagioclase with Na, Fe, Al pyroxene, a mineral with a composition similar to yagiite (silicate with hexagonal silicate ring). Inclusion IIAB D1 i4 consists mostly of glassy matrix with a large crystal of Ca phosphate 0.07×0.23 mm in size at one edge. Chains of angular skeletal crystals of chromite from 0.018×0.013 mm to 0.045×0.050 mm in size with cores of glassy materials are distributed from the Ca-phosphate crystal to the metal grain boundary (Fig. 2d). Three rounded grains of troilite are present close to the phosphate crystals and chromite. The texture suggests that chromite crystals grew rapidly before the melt was quenched to glass. Inclusion CF1F i8 is a complex quadrilateral inclusion consisting of Na plagioclase, albitic glass, troilite, and a pyroxene-like phase with a composition between kosmochlor, diopside, and Na-Ti-(Fe, Mg) pyroxene (Fig. 3b). More mineralogical and crystallographic studies are required to be sure of the presence of the solid solution series between the above end members.

3.2. Mineralogy of the Surface Inclusion

This inclusion was originally described as a large sanidine crystal more than 10 cm long (Wasserburg et al., 1968). We made a new thin section of this inclusion (PTS C1 LF). This PTS also contains K feldspar as a major phase, but orthopyroxene and Cr diopside are abundant along with minor nodules of olivine. The new section represents a region richer in mafic minerals. The major occurrence of K feldspar in the new thin section is an irregular veinlike region in contact with large orthopyroxene crystals, thickened in some parts (Fig. 3c). This large K feldspar is the same as sanidine described by Wasserburg et al. (1968). Silica is present within this K-feldspar region. Large single crystals of orthopyroxene and subrounded Cr diopside were found with K feldspar. Orthopyroxene occurs as a large transparent single crystal, often surrounded by healed fractures. Dusty cores have clear rims. Within the central dusty portion bound by healed fractures, tiny euhedral transparent crystals of K-Na feldspar are abundant (Fig. 2e). Their compositions are more sodic than the major K feldspar. Chromite inclusions slightly larger than the feldspar inclusions are also present in the clear orthopyroxene crystal. The dusty cores also include diopside. Rounded Cr diopside with exsolution texture similar to IIABD1 i1 (Fig. 2f) is present in contact with orthopyroxene and K feldspar. Olivine has been described previously in a separate surface inclusion (Wasserburg et al., 1968), but the new PTS shows a good textural relationship of olivine with the major minerals. Two deformed-oval-shaped olivines occur in orthopyroxene partly rimmed by irregular veins of K feldspar. A mineral distribution map (produced from elemental maps of Si, Ca, K) around a rounded olivine shows their detailed textural relationships (Fig. 3c). Rounded lath-shaped K feldspar including small orthopyroxene crystals also occurs in the center of the olivine inclusion (Fig. 3c).

3.3. Chemical Compositions of Minerals

The major silicate minerals in the interior Colomera inclusions, Na plagioclase and Cr diopside, exhibit a small range of compositions (Figs. 4 and 5; Tables 2 and 3). Sodic plagioclase in interior inclusions ranges in composition from $Or_{2.5}Ab_{90.0}An_{7.5}$ to $Or_{3.5}Ab_{96.1}An_{0.4}$ or to $Or_{5.4}Ab_{92.0}An_{2.6}$ (Table 2, Fig. 4b). Variations are observed both from core to rim and from grain to grain. In a few inclusions (e.g., CF1F i11), small crystals of K feldspar are attached around a large Na-plagioclase crystal. Rare plagioclase crystals (e.g., C1-3 fragment) show antiperthite texture and the compositions of the host ($Or_{92.4}Ab_{7.5}An_{0.1}$) and lamellae ($Or_{2.9}Ab_{96.6}An_{0.5}$) phases are widely separated. Chromium diopside ranges in compositions from $Ca_{44}Mg_{48}Fe_8$ to $Ca_{35}Mg_{42}Fe_{23}$ (Table 3, Fig. 5). Many crystals are slightly zoned and within one grain the chemical composition can vary from Ca-, Mg-rich to Ca-, Mg-poor (e.g., $Ca_{44}Mg_{46}Fe_{10}$ to $Ca_{40}Mg_{43}Fe_{17}$). The chemical compositions of Cr diopside and orthopyroxene of the surface inclusion differ only in small degree from those of the interior inclusions.

Chromium-diopside crystals in IIABD1 (Fig. 2c) are rarely

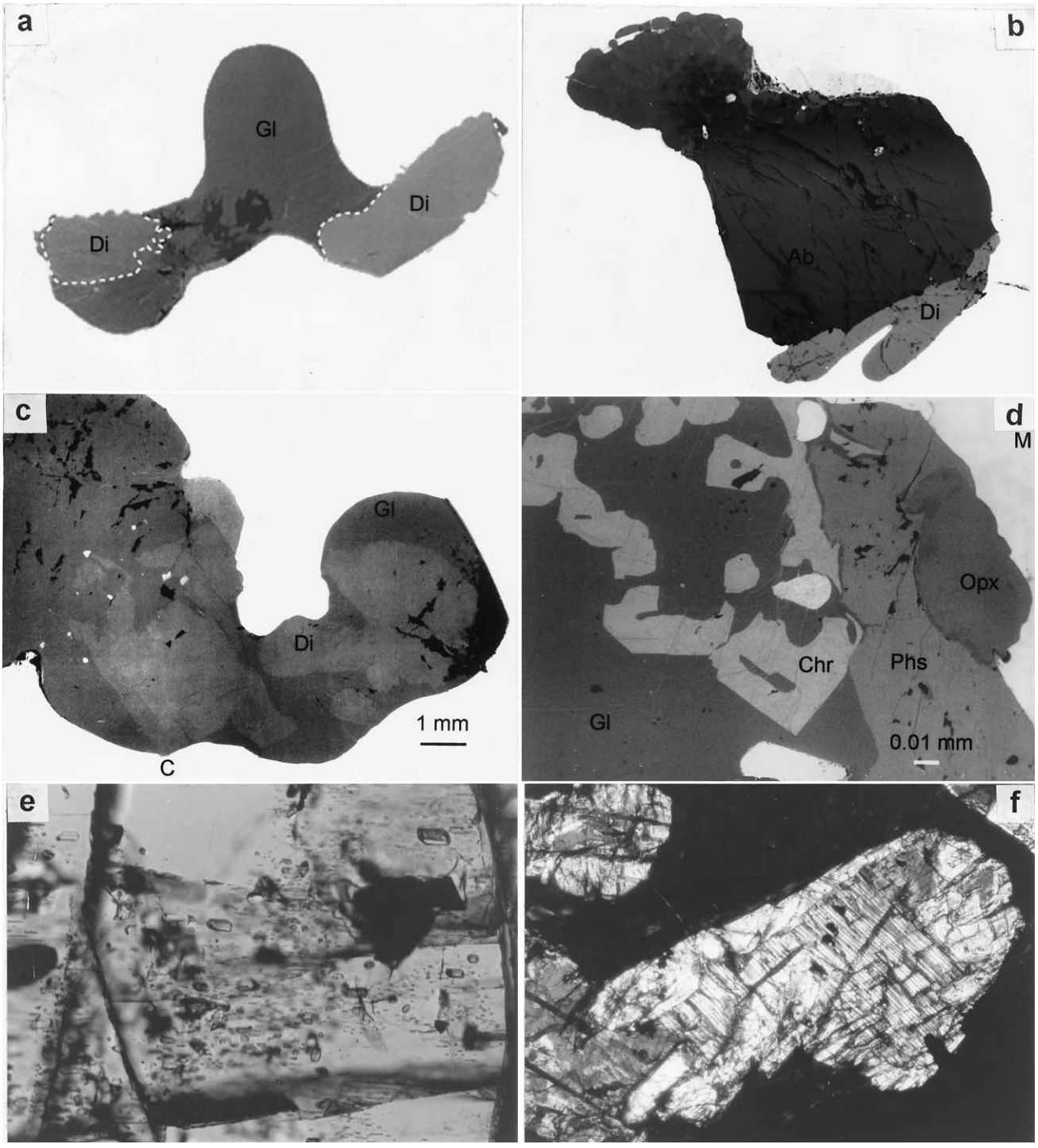

Fig. 2. Photomicrographs and back-scattered electron images (BEI) of Colomera. (a) An octopus-shaped CF1F i12 with a rounded glassy head (Gl) and two legs of angular diopside crystals (Di). BEI. The longest size is 2.3 mm. (b) A penguin-like CF1F i11 inclusion with a body of Na plagioclase (Ab), two legs of Cr diopside (Di), and a head of mixtures of two minerals and tiny K-feldspar crystals. BEI. The longest size is 2.3 mm. (c) Angular metal–pyroxene boundary of silicate inclusion (C), Colomera IIABD1 i1. Metal–glass boundary (Gl) is rounded. Scale is indicated by bar. BEI. (d) Skeletal chromite crystals (Chr) grown in glass (Gl) adjacent to a large Ca-phosphate crystal (Phs) in Colomera IIABD1 i4. Opx = orthopyroxene; M = metal. Scale is indicated by white bar BEI. (e) Tiny euhedral crystals of K-Na-feldspar in a large clear orthopyroxene crystal in PTS C1LF. Width is 1.3 mm. (f) Photomicrograph of Cr diopside (light gray with striations) in the IIABD1 i1 inclusion. The grain is marked as Di in Figure 2c. Diopside is rimmed by orthopyroxene (white) enclosed in glass (top dark area) and facing the metal wall (lower right dark area). Width is 2.2 mm.

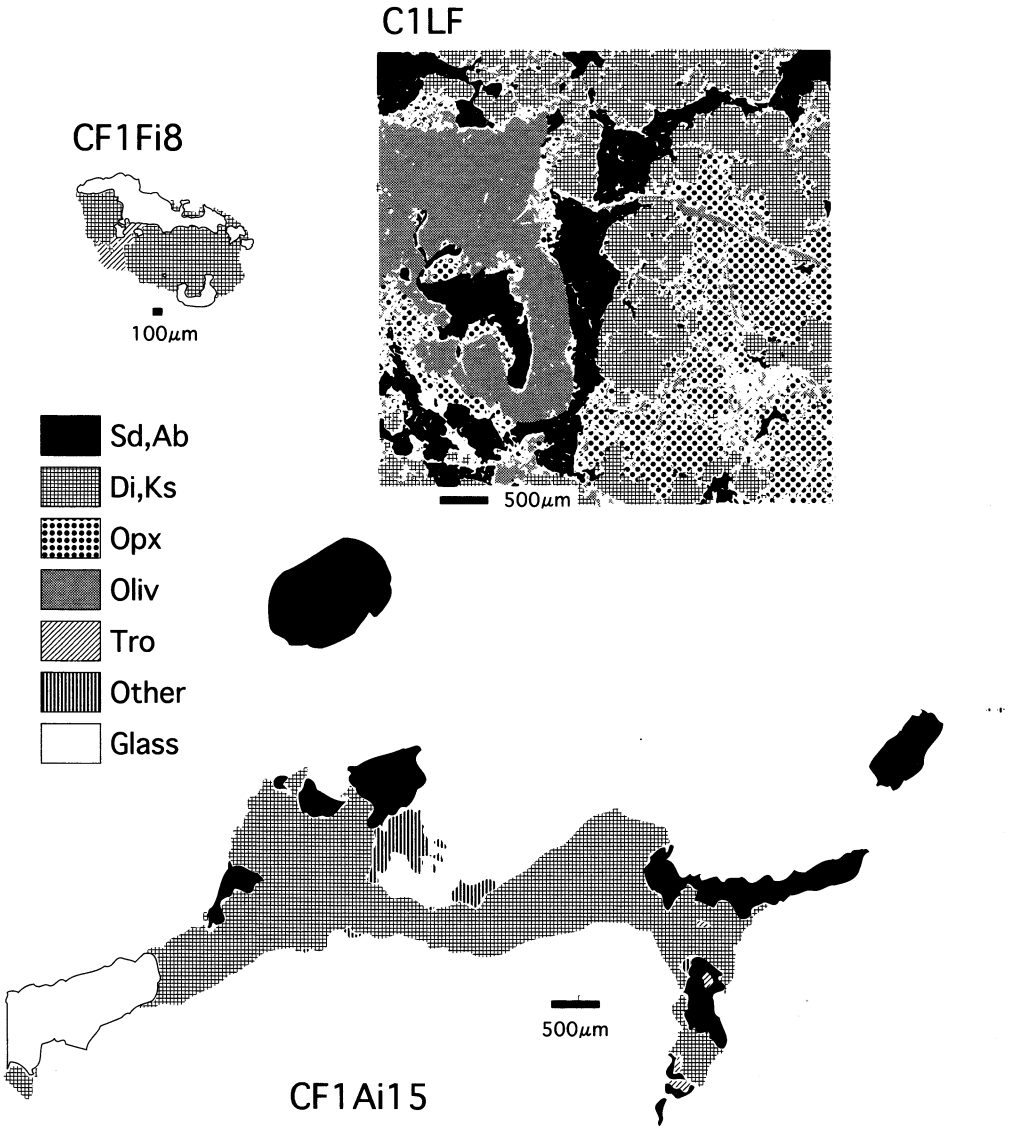

Fig. 3. Mineral distribution maps of (a) sections CF1A i15 and (b) CF1F i8, and (c) the large surface inclusion, PTS C1 LF. Patterns of sanidine (Sd) in C1 LF, Na plagioclase (Ab) in CF1Ai15, diopside (Di) in C1 LF, CF1Ai15, Na-Cr-Al-Ti pyroxene (Ks) in CF1Fi8, orthopyroxene (Opx), olivine (Oliv), troilite (Tro), glass, and others are shown in the figure.

partly skeletal and have thin rims of orthopyroxene. The orthopyroxene forming rims on Cr diopside has nearly constant chemistry (Fig. 5). The Cr-diopside crystals may also show fine exsolution-like lamellae textures on (001), such as in IIABD1 i1 (Fig. 2f). The partly skeletal crystal includes some glass, which also contains tiny chromite crystals. In a tubelike glassy inclusion ~0.01 mm in diameter, there is a needlelike core of chromite (Fig. 2c). The mineral assemblage and texture indicate that chromite crystallized from the melt, which was quenched to retain glassy appearance. Chromites in glassy inclusions (Table 4) are rich in Al.

A few interior inclusions contain pyroxenes apparently in the solid solution series between kosmochlor, diopside, and Na-Ti-pyroxene with fair amounts of Ti (Table 5). Crystal chemistry of the kosmochlor-diopside solution based on synthetic samples assures the existence of such solid solution (Ohashi and Fujita, 1979; Ohashi et al., 1982). Recently, diopsidic pyroxene with some kosmochlor components has been found in terrestrial rocks (Sakamoto and Takasu, 1996).

Chemical compositions of glass interior inclusions vary over a relatively small range ($Or_{12}Ab_{84}An_3$ to $Or_7Ab_{90}An_2$, Tables 6 and 7). The range within one inclusion is comparable to that from one inclusion to another (e.g., Fig. 6). The variation trend plotted in the Or-(Ab + An)-Qz diagram (Fig. 7) is limited along (Ab + An) to quartz edge. However, compositions of glasses related to mafic silicates vary widely. The Ca content of the glass is lower at the contact with Cr diopside (An_0 to $An_{0.5}$), consistent with growth of pyroxene from the glass. Glass in contact with whitlockite has a high Ca concentration (An 9.7 to 12.7), which implies that phosphate is dissolving into the glass.

Chlorapatite contains very low amounts of other cations,

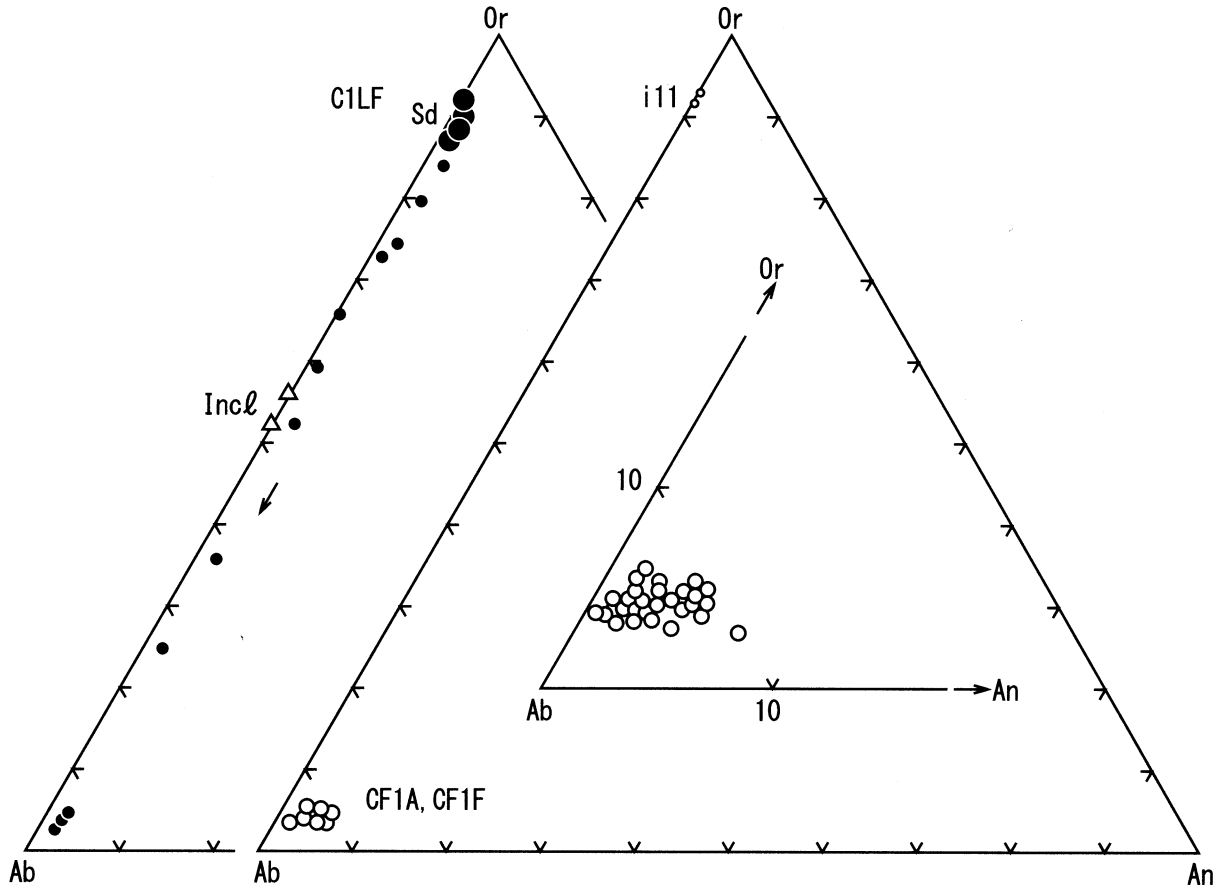

Fig. 4. Chemical compositions of alkali–feldspar in silicate inclusions of Colomera plotted in the Or-Ab-An diagrams. (a) C1LF surface inclusion (left). Sd = sanidine crystals in C1LF; allow = zoning trends toward the top of the Na-rich nodules; Incl = tiny euhedral inclusions in orthopyroxene. (b) CF1A, CF1F interior inclusions (right). *i*11 indicates tiny K feldspar around an albite crystal of CF1F i11. Compositions of albite around the Ab corner are enlarged for CF1A, F.

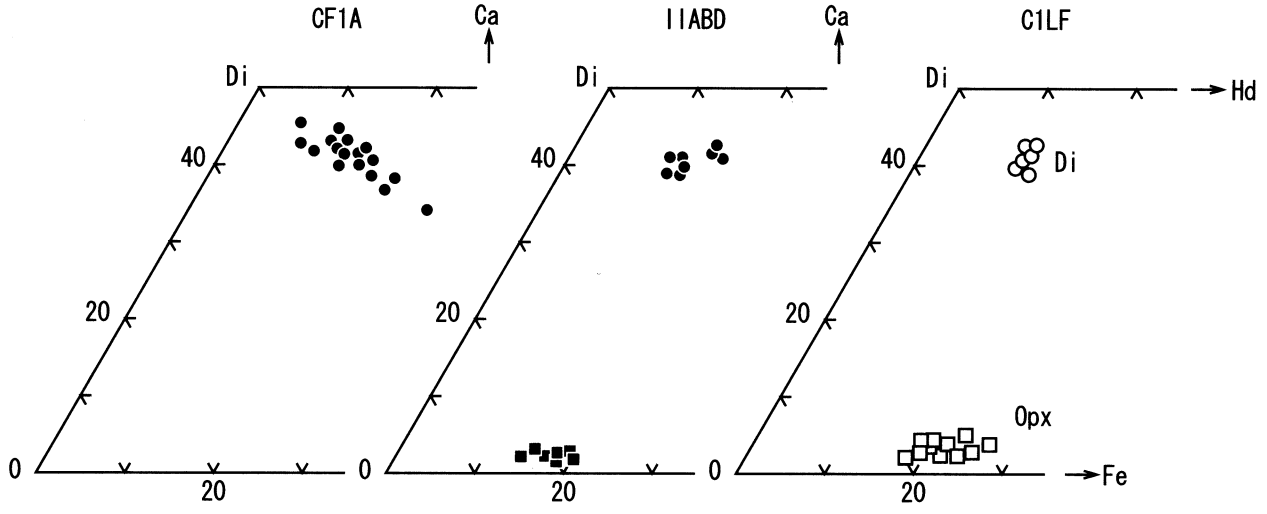

Fig. 5. Chemical compositions of pyroxenes (mol%) in silicate inclusions, CF1A, IIABD1, C1LF of Colomera plotted in parts of the pyroxene quadrilaterals. Opx = compositions of orthopyroxene; Di = diopside.

Table 2. Chemical compositions (wt%) of Na plagioclase in inclusions in slice CF1A of Colomera.

Inclusions	Ai1	Ai3	Ai6	Ai15	Ai18	Ai25
Mode[a]	0.69	0.43	0.85	0.2	0.73	0.24
SiO_2	67.77	68.01	67.83	68.36	67.64	68.30
TiO_2	0.11	0.12	0.08	0.15	0.11	0.17
Al_2O_3	20.22	19.98	19.94	19.83	19.48	19.36
FeO	0.29	0.37	0.10	0.26	0.60	0.52
MnO	0.01	0.00	0.00	0.01	0.03	0.03
MgO	0.00	0.00	0.03	0.01	0.01	0.02
CaO	0.75	0.61	0.70	0.60	0.51	0.34
Na_2O	10.77	10.86	10.70	10.12	10.70	10.79
K_2O	0.74	0.80	0.68	1.21	0.78	0.70
Cr_2O_3	0.03	0.04	0.04	0.03	0.00	0.05
Total	100.70	100.79	100.09	100.57	99.85	100.26

[a] Mode: estimated modal abundance (vol. fraction) of plagioclase in an inclusion.

except for Na. The Na content is 0.37 to 0.39 for 56 oxygens, whereas whitlockite contains 1.84 to 2.00 Na and 1.90 to 1.98 Mg/56 oxygens (Table 8). Chemical compositions of other accessory minerals (e.g., rutile) are given in Table 4.

The chemical compositions of some minerals of the surface inclusion differ from those of the interior inclusions. Potassium feldspar in the large surface inclusion shows little variation, ranging from $Or_{92.7}Ab_{7.2}An_{0.1}$ to $Or_{87.3}Ab_{11.0}An_{1.7}$ (Fig. 4a, Table 9). However, some enrichments of the albite component (Ab1 in Table 9) have been detected at the end of curved elongated nodules intruded into the mafic silicates. The euhedral alkali-feldspar inclusions in a large single-crystal orthopyroxene coexisting with K feldspar have a composition in the middle of the solid solution series ($Or_{51}Ab_{48}An_{0.1}$) (Na-K Fd in Table 9 and Fig. 4a). The large single crystal of orthopyroxene is zoned from $Ca_{1.3}Mg_{80.5}Fe_{17.8}$ to $Ca_{3.1}Mg_{78.1}Fe_{18.9}$(Table 10). Note that compositions of orthopyroxene and Cr-diopside crystals in all of the inclusions are nearly the same regardless whether they coexist with Na plagioclase (interior inclusions) or sanidine (surface inclusion). Olivine was detected only in the surface inclusion. Most of the olivines are chemically zoned. The composition of one crystal ranges from Fo_{67} to Fo_{76}, and another grain is zoned from Fo_{64} to Fo_{71} (Table 11).

3.4. Bulk and Trace Element Compositions of Inclusions

Bulk chemical compositions of six of the larger interior inclusions (Table 12) were estimated from the modal abundances of minerals and glass, their densities, and weighted mean compositions for each mineral as analyzed by EPMA (Tables 2 to 4, 6 to 8). The modal abundances (Table 12) were estimated from the areas of component minerals in the mineral distribution maps (see Experimental Methods). The bulk compositions (Fig. 8) show some variability, as would be expected from the differences in modal mineralogy (Tables 1 and 12).

The abundances of REEs in the various phases of Colomera were reported previously (Hsu et al., 1997; data presented in table form in Takeda et al., 2002). For the most part, all feldspar grains measured, regardless of location, have similar patterns and REE concentrations (Fig. 9) despite large variations in textures, modes, and bulk compositions for the inclusions. This is also true for olivine and diopside and, in most cases, for orthopyroxene (Fig. 9). Feldspar and glass have significant positive Eu anomaly, whereas diopside, orthopyroxene, and most phosphates have negative Eu anomalies, consistent with partitioning among phases in an igneous system.

Table 3. Chemical compositions (wt%) of diopsides in Colomera silicate inclusions.[a]

Inclusion	Ai1	Ai3	Ai6	Ai15	Ai18	Ai25	IIABD1i1	C1 LF	C1 LF
Mode[b]	0.31	0.57	0.08	0.66	0.22	0.76			
Remarks	Ave	Ave	Ave	Ave	Ave	Ave	Ave	Core	Rim
SiO_2	52.63	53.07	53.32	53.35	54.17	53.88	53.60	53.56	53.79
TiO_2	0.58	1.02	1.42	1.08	1.20	0.32	0.34	0.35	0.67
Al_2O_3	0.96	0.69	0.38	0.58	0.44	1.00	0.93	0.77	0.44
FeO	6.87	6.41	6.39	7.51	6.24	7.23	7.22	7.04	6.59
MnO	0.37	0.43	0.38	0.41	0.39	0.40	0.48	0.50	0.60
MgO	14.97	15.07	14.32	14.73	14.67	15.81	16.49	16.37	16.17
CaO	20.31	19.74	18.85	18.83	19.57	18.96	19.43	18.84	18.23
Na_2O	0.84	1.07	1.46	1.29	1.24	0.65	0.55	0.69	1.02
K_2O	0.02	0.02	0.01	0.02	0.01	0.01	0.02	0.00	0.01
Cr_2O_3	1.61	1.76	2.22	2.02	1.92	1.32	1.18	1.29	1.69
P_2O_5	0.00	0.00	0.02		0.00	0.00		0.00	0.02
Total	99.16	99.28	98.75	99.82	99.82	99.58	100.23	99.46	99.32

[a] Ai1 to Ai25 are inclusions in Slice CF1A. Core and rims are analysis of a grain.
[b] Mode = estimated modal abundance (vol. fraction) of diopside in an inclusion; Ave. = average.

Table 4. Chemical compositions (wt%) of chromites in the Colomera silicate inclusions.

Sample	IIABD1	IIABD1	IIABD1	IIABL1	CF1A	C1LF	IIABD1
Inclusion	i4	i4	i4	i5	i18		i5
Remarks	Core	Rim	Adj/glass[a]		Grain	In Opx	Rutile
Anal. No.	16–25	11–28	13–27	340–1	35,243	319–20	37
SiO_2	0.02	0.02	0.03	0.02	0.07	0.03	0.01
TiO_2	1.61	1.49	1.53	1.91	4.79	0.82	99.80
Al_2O_3	19.12	19.47	19.31	16.05	2.67	5.75	0.01
FeO	22.86	22.68	22.88	21.71	24.34	26.15	0.56
MnO	1.79	1.82	1.79	1.80	1.90	1.01	0.00
MgO	7.70	7.74	7.67	8.02	5.18	4.83	0.01
CaO	0.00	0.00	0.01	0.02	0.04	0.00	0.01
Na_2O	0.03	0.03	0.02	0.02	0.06	0.01	0.01
K_2O	0.01	0.01	0.02	0.03	0.04	0.02	0.02
Cr_2O_3	47.88	47.46	47.31	50.09	59.26	61.52	0.20
Total	101.02	100.71	100.55	99.63	98.33	100.12	100.65

[a] Adj/glass = adjacent to glass.

However, the REE contents of glass and phosphates vary considerably among inclusions (Fig. 9), and at least one orthopyroxene differs significantly from the others. The bulk REE abundances for the inclusions are similar to those found by previous investigators in other silicate inclusions in IIE iron meteorites (Ikeda et al., 1997b; Ruzicka et al., 1999) and in acapulcoites/lodranites (Floss, 2000). The sanidine crystals in the C1LF surface inclusion have almost the same REE concentrations as the Na-plagioclase grains in the interior inclusions (CF1A i3, i4, i6; Fig. 9). Olivine grains in C1LF, the sanidine-bearing inclusion, have low REE abundances and patterns depleted in light REEs. Late-forming phases, such as phosphate, orthopyroxene, and glass, often exhibit significant Yb anomalies, both positive and negative (Fig. 9). These anomalies

Table 5. Chemical compositions (wt%) of pyroxene-like phase rich in Na, Cr, Ca, Mg, and Ti in a Colomera silicate inclusion, CF1F i6.

Anal. No.	115	116	117	118	122	123	124
SiO_2	53.9	54.35	54.2	54.37	53.85	53.11	53.8
TiO_2	5.75	5.64	5.95	5.7	5.92	5.54	5.91
Al_2O_3	0.18	0.18	0.19	0.2	0.17	0.21	0.22
FeO	2.57	2.29	2.53	2.33	2.42	3.48	2.55
MnO	0.35	0.31	0.24	0.36	0.31	0.28	0.29
MgO	8.25	8.04	7.27	7.87	7.8	7.82	7.53
CaO	9.95	9.75	8.72	9.72	9.35	9.64	8.85
Na_2O	7.63	7.75	8.32	7.66	8.02	7.64	8.12
K_2O	0.02	0	0	0	0.01	0.04	0.03
Cr_2O_3	11.05	10.74	11.95	11.08	11.62	11.05	11.86
Total	99.65	99.06	99.39	99.29	99.48	98.82	99.16

Table 6. Chemical compositions (wt%) of sodic glass in the Colomera inclusions.

Inclusion	CF1Ai6	CF1Ai15	CF1Ai16	CF1Ai10	CF1Fi7	IIABGFi1
Anal. No.	264	44	62	266	Ave of 4	330
Mode[a]	0.02	0.12	1	1	1	1
SiO_2	67.35	66.46	67.64	68.98	72.47	74.67
TiO_2	0.06	0.27	0.03	0.18	0.74	0.35
Al_2O_3	18.64	17.62	20.12	18.66	13.97	17.38
FeO	1.86	1.85	0.07	0.34	0.97	0.11
MnO	0.21	0.07	0.01	0.00	0.03	0.02
MgO	0.00	1.31	0.00	0.06	0.39	0.11
CaO	0.07	2.20	0.82	0.01	0.04	0.78
Na_2O	10.99	9.84	10.69	10.87	8.68	5.18
K_2O	0.70	0.94	0.76	0.68	1.91	1.06
Cr_2O_3	0.00	0.24	0.00	0.00	0.03	0.00
Total	99.88	100.80	100.14	99.79	99.21	99.66

[a] Mode = modal abundance of glass in an inclusion.

Table 7. Chemical compositions of glassy materials in the Colomera inclusion i1 in PTS IIABD1.

Inclusion	i1	i1	i1	i1	i1	i4
Remarks[a]	Di-Fe	Rim	w/Di	w/Di Bulk	In Opx	w/chrom.
No.[b]	13	5	3	6	5	1
SiO_2	72.2	72.6	76.3	72.1	72.4	69.7
TiO_2	0.31	0.34	0.03	0.29	0.44	0.42
Al_2O_3	16.53	16.42	11.79	16.36	16.43	17.13
FeO	0.20	0.33	1.07	0.38	0.13	0.16
MnO	0.05	0.01	0.04	0.03	0.05	0
MgO	0.09	0.05	0.03	0.04	0.12	0.14
CaO	0.34	0.28	0.39	0.34	0.35	0.59
Na_2O	8.63	8.91	3.65	8.83	8.72	9.11
K_2O	1.04	1.04	4.79	1.08	1.05	1.04
Cr_2O_3	0.04	0.01	0.08	0.04	0.01	0
Total	99.43	100.00	98.16	99.52	99.64	98.30

[a] Di-Fe = glass between diopside and FeNi-metal; w/Di = glass with diopside; w/chrom = with glass with chromite.
[b] No. = numbers of measurements.

are not seen in diopside, olivine, and feldspar. Some glasses and one olivine also appear to show negative Sm anomalies (Fig. 9). These anomalies may be artifacts of the analysis procedure. Particularly in the case of olivine, count rates are so low that one count can make a major difference in the result.

4. DISCUSSION

Since the discovery of K-feldspar-rich inclusions in Colomera (Wasserburg et al., 1968), the number of silicate-bearing IIE irons has increased to eight (Olsen et al., 1994). Bunch et al. (1970) recognized that Weekeroo Station, Colomera, and Kodaikanal form a group. The diversity of silicate inclusion types among the IIEs now enables us to discuss various models proposed for their origin. Although the mineral assemblages of Colomera (Wasserburg et al., 1968), Kodaikanal (Bunch and Olsen, 1968), and Elga (Osadchii et al., 1981) are highly fractionated, some IIE irons, such as Netschaëvo, contain angular chondritic inclusions (e.g., Bild and Wasson, 1977). The broad range of ages is another interesting feature of the IIE irons. The Rb-Sr age of Colomera, 4.51 Ga (Sanz et al., 1970), is the oldest, and ages of Kodaikanal, 3.5 to 3.7 Ga, are among the youngest (Burnett and Wasserburg, 1967; Bogard et al., 1969). Mineralogical characterization of age-dated inclusions is essential in interpreting the formation mechanism and ages of IIE irons.

As discussed in the introduction, a range of models has been proposed for the origin of IIE irons. The IIE irons are considered to have a nonmagmatic origin in the original classification of the iron meteorites (Scott and Wasson, 1976). The O-isotope compositions of IIE silicates and H chondrites are very similar (Clayton et al., 1983), which suggests a genetic relationship. One of the basic problems of origin of IIE irons is how to produce the alkali-rich materials found in the inclusions from

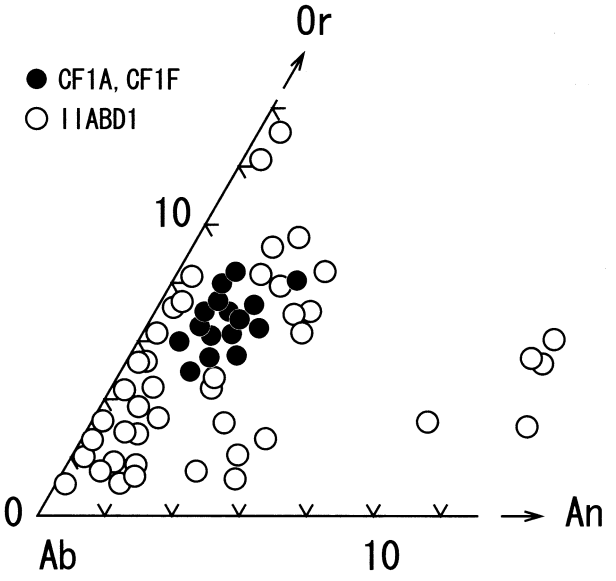

Fig. 6. K-Na-Ca compositions of albitic glass in the colomera inclusions (CF1A, CF1F, IIABD1) plotted in parts of the Or-Ab-An diagrams.

Table 8. Chemical compositions (wt%) of Ca phosphates in the Colomera silicate inclusions.

	Cl-apatite		Whitlockite	
Sample	CF1A	CF1A	CF1A	CF1F
Inclusion	i6	i6	i5	i13
Remarks	Core	Rim		
Anal. No.	4,5	6	27–29	110
Na_2O	0.48	0.51	2.61	2.54
MgO	0.01	0.00	3.50	3.49
Al_2O_3	0.00	0.00	0.00	0.00
SiO_2	0.06	0.02	0.03	0.05
K_2O	0.00	0.00	0.00	0.00
CaO	51.5	52.4	45.8	45.5
TiO_2	0.01	0.01	0.00	0.00
Cr_2O_3	0.00	0.00	0.04	0.00
MnO	0.00	0.00	0.04	0.04
FeO	0.13	0.45	0.53	0.95
P_2O_5	40.4	40.4	44.3	45.3
Cl	5.61	5.61	0.01	0.01
Total[a]	98.21	99.40	96.85	97.81

[a] O equivalent to Cl is not subtracted.

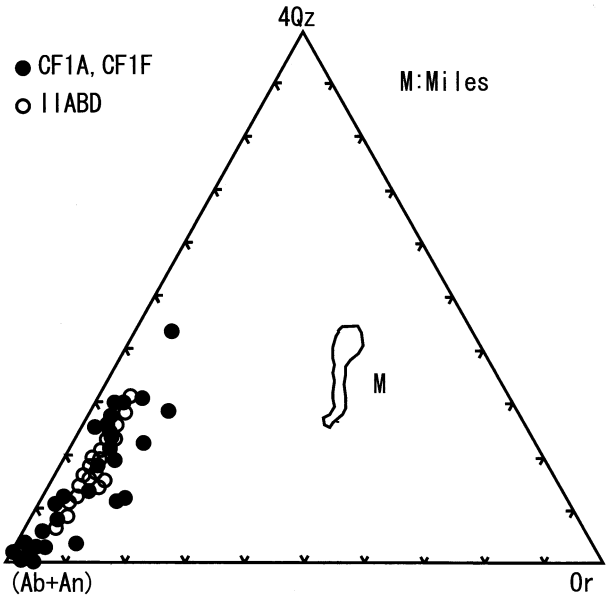

Fig. 7. Chemical compositions of albitic glass plotted in the quartz-plagioclase(Ab + An)-orthoclase(Or) diagram. The modal quartz contents (Qz) were calculated by equation Qz = Si − 3(K + Na) − 2Ca − (Mg, Fe, Mn) Atomic % for O = 24. M = granitic glass in Miles (Ikeda and Prinz, 1996).

an H-chondrite-like source material. Partial melting of a chondritic precursor has been proposed to explain primitive achondrites, such as acapulcoite/lodranite and winonaite/IAB silicate inclusions on the basis of mineralogical studies (McCoy et al., 1997; Takeda et al., 1994, 2000). However, the chemical composition of small degrees of partial melt is not well enough understood to be applied to IIE problems because of the influence of many minor elements in the multicomponent system. Plagioclase-diopside-rich andesitic material discovered in IAB irons (Takeda et al., 1994, 1997, 2000) gives us a hint of what the first partial melts of near chondritic material might look like.

4.1. Origin of Colomera Silicates

A remarkable observation concerning the 48 interior inclusions is that the two most abundant minerals, Na plagioclase and Cr diopside, have limited ranges of composition. The coexisting glasses have near Na-plagioclase compositions with excess silica. The reason why we have more silicic melt can be seen in the diopside-albite-SiO_2 system (Fig. 10) redrawn from the diopside-nepheline-SiO_2 system (Schairer and Yoder, 1960). In this figure, plagioclase has minimum melting temperature at 1062°C toward the SiO_2 side. The phase boundary between diopside + liquid and plagioclase + liquid is at around 1100°C. Thus, over a wide range of bulk chemical compositions, the mineral assemblage observed in the inclusions can exist. The close similarity in the compositions of crystalline plagioclase and albitic glass can be explained by the presence of plagioclase + liquid field around 1100°C at the albite end member.

However, a rough average of bulk compositions based on modal abundances (Table 12) contains ~4% FeO and implies that the melt that gave rise to the inclusions does not lie on the diopside-plagioclase join shown in Figure 10. Colomera pyroxenes contain Fe and have Fe/(Mg + Fe) mole ratios = 0.2. Albite is Or ~5 and An ~8. The influence of these minor elements and the presence of minor orthopyroxene should be taken into account for more detailed discussion. The best information on the topology of the augite liquidus surface for a basaltic composition is provided by a phase diagram in the olivine-plagioclase-wollastonite-quartz model system parameterized by Longhi (1991).

The evolutionary path of the partial melt of the H chondrites has been discussed by Ruzicka et al. (1999) on the basis of a plot of the bulk composition of H chondrites on the olivine-plagioclase-quartz model system (Fig. 9 of Ruzicka et al., 1999) for a composition with Mg# = 0.70, normative albite N_{Ab} = 0.50, and normative orthoclase N_{or} = 0.05. To compare the peritectic with the average composition of the inclusions and to show how that melt evolves, we need a diagram for more Na- and Mg-rich composition.

A diagram of the olivine(Ol)-plagioclase(Pl)-quartz (Qz) di-

Table 9. Chemical compositions (wt%) of alkali feldspars in C1 LF of Colomera.

Minerals[a]	Sd1	Sd1	Sd2	Sd3	Ab1	Na-K Fd
Remarks	Outer	Inner	Inner	Or1	Rim	Inclusion
SiO_2	64.72	64.54	65.01	64.86	67.91	70.66
TiO_2	0.06	0.08	0.10	0.07	0.11	0.18
Al_2O_3	18.45	18.60	18.50	18.13	19.16	16.24
FeO	0.06	0.10	0.09	0.11	0.12	0.43
MnO	0.02	0.01	0.02	0.00	0.00	0.00
MgO	0.00	0.00	0.00	0.00	0.00	0.01
CaO	0.06	0.13	0.03	0.04	0.41	0.00
Na_2O	0.98	1.03	0.95	0.98	11.71	4.08
K_2O	15.32	15.29	15.21	15.10	0.69	7.49
Cr_2O_3	0.00	0.01	0.02	0.01	0.03	0.05
V_2O_3	0.01	0.02	0.01	0.01	0.00	0.00
NiO	0.01	0.01	0.01	0.01	0.00	0.00
P_2O_5	0.03	0.04	0.02	0.02	0.03	0.10
Total	99.73	99.85	99.97	99.34	100.17	99.24

[a] Sd = sanidine; Ab = albite; Na-K Fd = small feldspar crystal in orthopyroxene.

Table 10. Chemical compositions (wt%) of orthopyroxene (Opx) in the Colomera silicate inclusions.

Inclusions	IIABD1 i5	IIABD1 i1	C1LF				
Crystal	Opx1	Opx1	Opx1	Opx1	Opx1	Opx2	Opx2
Remarks			Clear rim	ar/Fd[a]	Dusty core	Clear rim	Dusty core
SiO_2	55.53	54.88	55.6	55.39	54.47	55.43	54.88
TiO_2	0.31	0.39	0.05	0.12	0.2	0.05	0.14
Al_2O_3	0.65	0.98	0.25	0.4	0.67	0.29	0.41
FeO	12.25	11.58	12.2	11.95	9.58	12.37	13.25
MnO	1.63	1.67	0.57	0.56	0.53	0.54	0.69
MgO	28.43	28.51	28.72	28.78	22.61	28.5	26.98
CaO	1.51	0.82	1.28	1.33	9.19	1.28	2.18
Na_2O	0.08	0.02	0.12	0.11	0.65	0.15	0.22
K_2O	0.01	0.01	0.06	0.01	0.01	0	0.01
Cr_2O_3	0.36	0.42	0.65	0.68	1.54	0.72	0.78
V_2O_3			0.01	0.01	0.05	0.02	0.02
NiO			0.02	0.01	0.02	0.02	0.02
P_2O_5			0.01	0.01	0	0.01	0.01
Total	100.76	99.27	99.55	99.35	99.52	99.38	99.57

[a] ar/Fd = around K-Na feldsparthic inclusion.

agram for Mg# = 0.8, N_{Ab} = 0.9 and N_{Or} = 0.01 projected from augite (Fig. 8) has been constructed by using parameters and a program written by J. Longhi (1991) and modified by K. Saiki (personal communication, 1998) for comparison with the partial melt composition of chondritic source materials. With increasing N_{Ab}, the Ol-Pyx-Pl reaction point shifts to the right in Figure 8. The individual bulk compositions of six composite inclusions (Table 12) and the estimated bulk composition of all internal inclusions, deduced by averaging the six composite inclusions are plotted on Figure 8 following the projection equations in O units given by Longhi (1991).

The average bulk composition of composite Colomera inclusions plots near the peritectic point of Figure 8. The first melt for a composition in the Ol + Aug field, such as that of an H chondrite, will be at the peritectic (Ruzicka et al., 1999). The phase relationships of Figure 8 and the oxygen isotope data (Clayton et al., 1983) thus support partial melting of an H-chondrite-like material to produce the Colomera silicates. Our interpretation can be tested, by performing low-degree partial melting experiments on an H chondrite and extracting the lowest-melting fractions for chemical analysis. Support for a generally chondritic source comes from the average bulk REE patterns of the individual inclusions. The major minerals show compositions generally consistent with igneous partitioning (Fig. 9). A hypothetical bulk REE patterns for the original partial melt calculated from the modal abundances of minerals and their average REE concentrations is nearly flat. The average bulk REE composition of composite Colomera inclusions for Table 12, is six times the CI abundance. The expected pattern for a partial melt of chondritic material should be slightly enriched in light REEs. Uncertainties in the modal mineralogy of all inclusions make it difficult to identify this enrichment, but it is clear that the inclusions were not derived from a fractionated melt.

The bulk compositions of the individual composite inclusions listed in Table 12 form an array between the diopside-rich inclusion and plagioclase that cuts through the Pl + Aug (diopside for Colomera) and Lpyx + Aug fields (Fig. 8). This

Table 11. Chemical compositions (wt%) of olivine in a large silicate fragment, C1 LF rich in sanidine.

Minerals	Olivine 1	Large			Olivine 2	Small		
Remarks[a]	Rim	interm.	core	Ave.	Rim	interm.	core	Ave.
SiO_2	37.16	37.41	37.93	37.71	36.78	36.59	36.82	36.98
TiO_2	0.02	0.02	0.02	0.01	0.02	0.03	0.03	0.02
Al_2O_3	0.00	0.00	0.00	0	0.00	0.00	0.00	0.01
FeO	27.05	24.98	22.57	23.38	28.46	28.61	27.28	28.62
MnO	0.81	0.99	1.09	1.07	0.90	0.93	1.05	0.98
MgO	34.40	36.28	37.96	37.41	32.98	32.80	33.72	33.02
CaO	0.04	0.05	0.05	0.04	0.06	0.08	0.05	0.05
Na_2O	0.01	0.01	0.01	0.02	0.03	0.01	0.02	0.02
K_2O	0.01	0.01	0.00	0.01	0.00	0.01	0.01	0.01
Cr_2O_3	0.03	0.01	0.01	0.02	0.00	0.02	0.01	0.01
V_2O_3	0.01	0.01	0.01	0.01	0.01	0.01	0.01	0.01
NiO	0.04	0.05	0.03	0.02	0.02	0.03	0.02	0.03
P_2O_5	0.09	0.13	0.07	0.09	0.10	0.11	0.10	0.1
Total	99.68	99.94	99.77	99.79	99.34	99.23	99.13	99.85

[a] Core and rim are of one grain. Interm = intermediate between core and rim. Ave = average of entire grain.

Table 12. Bulk chemical compositions of larger inclusions in slice CF1A of Colomera calculated from modal abundance (vol. fract.) of minerals and their average composition.

Inclusion	Ai1	Ai3	Ai6	Ai15	Ai18	Ai25	Ave.
SiO_2	62.38	58.75	66.34	57.32	58.85	56.83	60.08
TiO_2	0.28	0.68	0.22	0.84	0.75	0.29	0.51
Al_2O_3	13.37	8.03	17.93	5.69	13.39	4.75	10.53
FeO	2.63	4.11	0.77	5.66	3.92	5.86	3.82
MnO	0.14	0.27	0.04	0.30	0.27	0.32	0.22
MgO	5.32	9.34	1.48	10.79	4.07	12.59	7.26
CaO	7.71	12.46	2.53	13.94	5.21	15.15	9.50
Na_2O	7.24	4.79	9.76	3.70	7.49	2.72	5.95
K_2O	0.48	0.31	0.61	0.32	0.53	0.15	0.40
Cr_2O_3	0.60	1.11	0.26	1.49	5.26	1.06	1.63
Total	100.15	99.85	99.95	100.05	99.73	99.72	99.91
Albite	0.69	0.43	0.85	0.2	0.73	0.24	0.52
Diopside	0.31	0.57	0.08	0.66	0.22	0.76	0.43
Glass	0	0	0.02	0.12	0	0	0.02
Apatite	0	0	0.04	0	0	0	0.01
Chromite	0	0	0	0	0.05	0	0.01

is consistent only with a simple mechanical mixing relationship, not a magmatic evolution series. The array of bulk compositions is due to differences in the proportions of plagioclase, diopside, and melt that either reflect the plane through which the inclusion was sampled or differences in the proportions of the three phases acquired when the inclusions were incorporate into the metal. If the variations in modal mineralogy are not artifacts of how the inclusion was cut, then for the inclusions to have originated from a single melt, the melt must have been partially crystallized and the individual inclusions formed from melt blobs with different amounts of crystals already present.

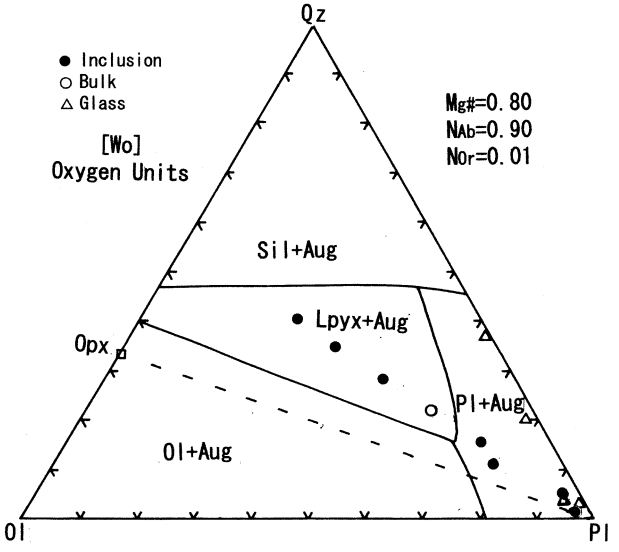

Fig. 8. A calculated bulk composition (Inclusion) of the silicate inclusions listed in Table 12 plotted in the quartz (Qz)–olivine(Ol)–plagioclase(Pl) diagram projected from augite using a program written by J. Longhi (courtesy of K. Saiki). The topology of the augite liquidus surface with composition $N_{Ab} = 0.9$, Mg# = 0.8, and $N_{Or} = 0.01$ are expressed by projection equations in oxygen units after Longhi (1991). Sil = silica, Aug = augite (diopside in Colomera), Ol = olivine, Opx = orthopyroxene, Lpyx = low-Ca pyroxene; bulk = average bulk composition of six composite inclusions; glass = compositions of some inclusions with only glassy material.

Compositions of several glassy inclusions are plotted as open triangles in Figure 8. The glass compositions lie along the quartz-plagioclase join and plot to the plagioclase side of the binary eutectic at Pl = 0.54. These compositions cannot be generated by equilibrium fractional crystallization of the composite inclusions. Instead, these inclusions appear to represent secondary melts of inclusions consisting primarily of plagioclase plus some diopside and silica that were separated from the main partly crystallized partial melt from the H-chondrite-like source during and after emplacement into the molten metal.

Because plagioclase has the lowest melting point of any of the minerals in the Colomera inclusions, we postulate that the plagioclase in the inclusions was partially remelted when the silicates were incorporated into the hot molten metal. Inclusions composed largely of plagioclase might melt to a large extent, whereas the inclusions composed largely of diopside would melt to a smaller degree because diopside melts at relatively high temperature. Inclusions that melted almost completely, those originally rich in plagioclase, would begin to crystallize plagioclase and the melt compositions would evolve toward the eutectic in the simple system of Pl-Qz-Aug (Pl = 0.54). Inclusions that quenched at various stages of crystallization would have melts that lie along the Pl-Qz join in Figure 8. This model would predict that the glass in glassy inclusions with compositions close to the binary-eutectic would either have relatively high concentrations of plagioclase crystals or had been separated from their source plagioclase crystals during incorporation into the metal, if they were originally derived from the partial melt of an H-chondrite parent. Some aspects of this model for producing glass compositions in Colomera are similar to that proposed by Ruzicka et al. (1999), and this process only works if the melted inclusions were low in mafic components. Ruzicka et al. (1999) also proposed that normative orthopyroxene in the melt could be partly removed by FeO reduction, which could take place during metal–silicate mixing.

If we do not postulate the above melting process, we have to consider a role of disequilibrium crystallization during rapid cooling of the melt. Because of the presence of diopside crystals as a nucleus of crystal growth, mafic silicate components in the melt would be consumed to grow diopside and orthopyrox-

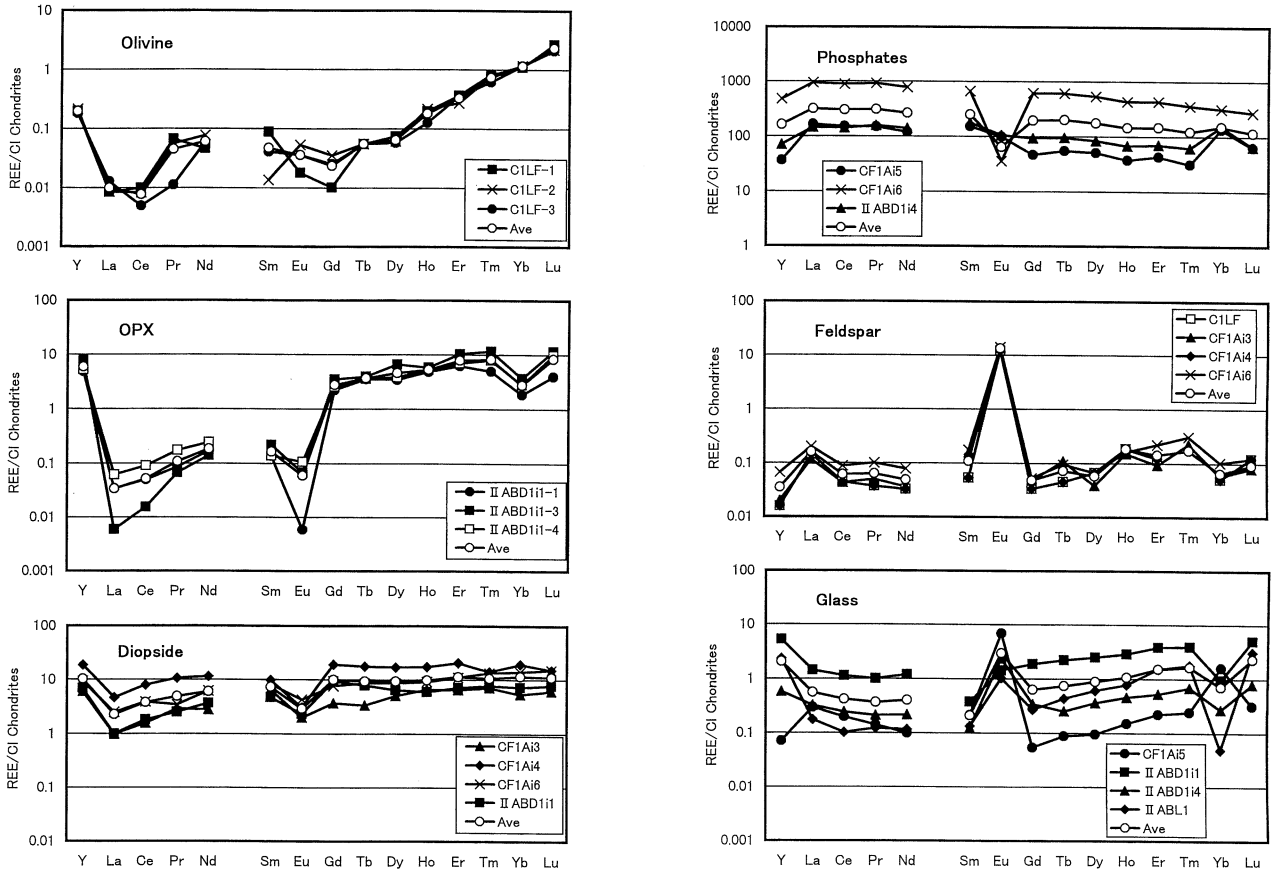

Fig. 9. CI-normalized abundances of trace elements in diopside, orthopyroxene, olivine (left), Ca phosphates, feldspars, and glass (right) in Colomera inclusions. Average values (Ave) for each mineral are shown by open circles. Olivine and feldspar C1LF (sanidine) are from the C1LF surface inclusion. The ion probe data are available at the Planetary Materials Database of Mineralogical Institute, University of Tokyo (Hsu et al., personal communication; Takeda et al., 2002)

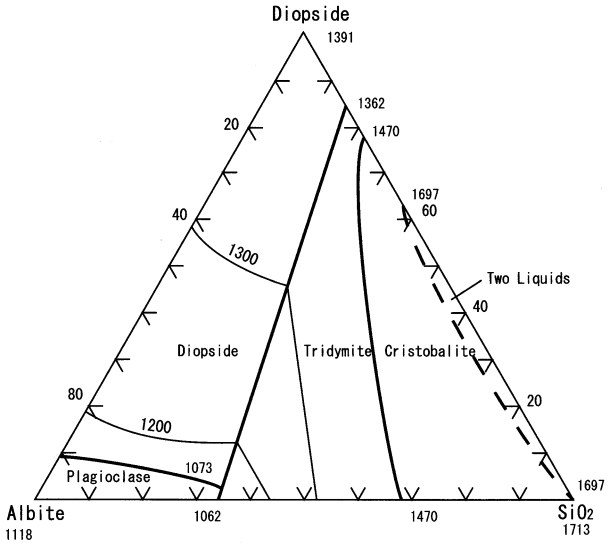

Fig. 10. The diopside–albite–SiO_2 system reproduced from the diopside–nepheline–SiO_2 system (from Schairer and Yoder, 1960).

ene on the existing crystals until the melt composition reaches to the plagioclase-quartz join. The melt would evolve away from plagioclase along the Pl-Qz join (Fig. 8) by the growth of Na plagioclase. Ruzicka et al. (1999) proposed a similar process of crystallization of pyroxene overgrowths on preexisting pyroxene, to explain glass compositions.

Mineralogical observations and chemical compositions of the inclusions are generally consistent with a two-stage model. The original melt derived from the H-chondrite-like source had already crystallized significant amounts of Cr diopside and Na plagioclase before it was dispersed and encapsulated by the partly molten metal. Ikeda et al. (1997a) described this as "crystal mush." The existence of crystal mush is shown by the coarse grain sizes of the diopside and plagioclase, their approximately uniform chemical composition across the suite of inclusions, the euhedral forms of diopside, the large variations in modal abundances of minerals and glass among the inclusions, and the angular boundaries between Cr-diopside crystals and the metal (Figs. 2a,c). Also, the irregular shapes of large inclusions may imply that the metal was also partially crystallized when it incorporated the silicate melt. The uniform chemical composition of minerals extends to a roughly constant abundance of REEs in diopside and albite, if we remove variations derived from local exchanges of REEs within an inclu-

sion. The crystal mush was somehow incorporated into molten metal, at which point some of the preexisting plagioclase crystals began to melt. As the metal-silicate mixture cooled, the silicate inclusions crystallized to some extent but were eventually quenched, leaving the residual liquid as glass. It was during this crystallization that the melt in the inclusions rich in the plagioclase component evolved away from plagioclase along the Pl-Qz join (Fig. 8).

4.2. Crystallization of Individual Inclusions

We have proposed that the Colomera inclusions originated from a single melt that was incorporated into the partly molten metal. However, each inclusion trapped a unique combination of mineral grains and melt, and after being engulfed by the molten metal, each inclusion evolved as a largely closed system. The facts that diopside REE patterns from many inclusions are very similar, feldspar REE patterns from many inclusions are very similar, and the two patterns are complementary support a hypothesis that they were already grown in the crystal mush before encapsulation in the metal (e.g., Hsu et al., 1997). Each inclusion has a unique bulk REE pattern that is controlled by the mixture of minerals in the inclusion. These bulk patterns were inherited from the original crystal mush and evolved as largely closed systems after incorporation into the metal.

Minor variations in major-element compositions within some individual diopside and plagioclase crystals, textural relationships and compositional variations within the glass and Ca phosphates, and the presence of several minor mineral phases are best interpreted in terms of crystallization within the inclusions. Very minor K feldspar was formed in a few interior inclusions around a large Na-plagioclase grain during the final crystallization stage (e.g., CF1F i11 in Fig. 4b). Orthopyroxene overgrowths are observed on Cr-diopside crystals (e.g., IIABD1 i1, Fig. 2f). Orthopyroxene is expected to crystallize from the peritectic composition in Figure 8 as it evolves to the eutectic. Crystallization of orthopyroxene may be enhanced by crystallization of Ca phosphates, which would deplete the melt in Ca and perhaps destabilize diopside. Some inclusions contain sizable grains of Ca phosphate. Some blocky phosphate grains may be primary because phosphorous is a plausible component of the first melts in chondritic material (e.g., McCoy et al., 1997). Chromite is as abundant as Ca phosphates in a few inclusions (IIABD1 i4), and their skeletal crystal forms suggest rapid growth within the inclusion (Fig. 2d). The high Cr contents of diopside and the presence of kosmochlor($NaCrSi_2O_6$)-diopside pyroxene in CF1F i8 indicate high Cr concentration in the melt. The larger ranges of the REE concentrations of glass and Ca phosphates can be explained by the growth of Ca phosphates within the inclusion. The REE compositions of the glass evolved by growth of minerals within the inclusion (Hsu et al., 1997). Some unusual REE concentrations in a particular inclusion can be explained by the growth of some minerals, but we will not discuss those local phenomena in this article.

The Yb anomalies, both positive and negative, found in various phases (Fig. 9) are unusual for magmatic rocks and may provide clues about the petrogenesis of individual inclusions. For the most part, negative Yb anomalies are found in the late-forming phases such as glass and orthopyroxene. Olivine and diopside show no anomalies and feldspar shows much subdued effects (Fig. 9). Thus, in a single inclusion, phases thought to be inherited from the crystal mush that predates mixing with metal are free of Yb anomalies (e.g., olivine, diopside, plagioclase) and phases that formed during or after mixing (orthopyroxene, some phosphates, glass) are depleted in Yb (e.g., Hsu et al., 1997). This indicates that Yb fractionation was somehow related to mixing of the crystal mush with molten metal. Hsu et al. (1997) considered distribution of REE during the growth of particular minerals within an inclusion. This redistribution would have occurred after individual inclusions were isolated from one another. However, we do not see complimentary Yb anomalies among phases of individual inclusions. To the contrary, most or all phases within an inclusion show anomalies of the same sign (Hsu et al., 1997). Ytterbium anomalies are most easily explained in terms of vapor-solid or vapor-liquid fractionation. Ytterbium, like Eu, is volatile under reducing conditions. This suggests that negative Yb anomalies might have been produced by evaporation under reducing conditions. However, evaporation of Yb would be accompanied by loss of other volatile elements such as Na. Some inclusions exhibit positive Yb anomalies, such as the phosphate-bearing inclusion studied by Hsu et al. (1997). Some of the phosphates in Colomera inclusions might have originated by oxidation of phosphorous from the molten metal. One possibility is that a volatile-rich gas generated from the crystal mush permeated the metal-silicate system during mixing. This gas acquired Yb, Na, and other elements from reduced inclusions, but the gas was not rapidly lost from the system. Some inclusions may have been undergoing active oxidation as phosphates formed from the molten metal. These inclusions might have extracted Yb from the gas phase. The net result was transfer of Yb from reduced to (relatively) oxidized inclusions while only a small fraction of the gas phase was lost from the system. This model minimizes evaporative loss of Na and other volatiles from the bulk system while permitting Yb to move between inclusions. The crystallization of the silicate inclusions within the metal apparently took place rather rapidly. For example, orthopyroxene rims on skeletal Cr-diopside crystals (e.g., IIABD1 i1) imply fairly rapid crystallization, as do the skeletal forms of chromite in some inclusions. The existence of various glass compositions between plagioclase and the binary eutectic, without the growth of acicular albite crystals, implies rapid cooling, but quenching is not required by the presence of glass alone. Glasses of silicic composition stay as glass for several years at 900 $\sim$ 1000°C in dry experimental runs (P. J. Wyllie, personal communication, 1998). Cooling must have slowed dramatically at temperatures below 500°C where the Widmanstätten pattern was developed.

4.3. Constraints for the K-Rich Surface Inclusion

The $<$10 cm long surface sanidine inclusion described by Wasserburg et al. (1968) has a much more K-rich composition than the interior inclusions located only a few tens of centimeters away. This extraordinarily high K content cannot be explained by the partial melting mechanism invoked to explain the low-K_2O interior inclusions, in which Na plagioclases retain K_2O/Na_2O wt % ratios comparable to those derived from chondrites (both $\sim$ 0.09). We will show below that the small K_2O/Na_2O variation trend of the glassy materials in the interior inclusions is inconsistent with an origin for the surface inclu-

sions by large-scale differentiation of the sodic melt or impact melting of the sodic glass. Small-scale concentration of K (Or_{91}) has been observed at grain boundaries of minerals within some Na-rich glassy inclusions (e.g., CF1F i11, i12).

The mafic silicates in the surface and interior inclusions have several features in common. Chromium diopside and orthopyroxene crystals are present in both types of inclusions. The common features for diopside and orthopyroxene include limited ranges of chemical composition and rounded shapes with fine lamella textures of diopside. In the large K-rich surface inclusion, ferromagnesian minerals are mostly enclosed by K feldspar in a poikilitic texture. Olivine grains also coexist with K feldspar and orthopyroxene in the surface inclusions (Fig. 3c). Textural and phase-equilibrium relationships show that the mafic silicates in the surface inclusion did not crystallize from the K-rich melt. A large orthopyroxene crystal appears to be invaded by thick, irregular, K-Si-rich, veinlike regions and a thickened part forms a sanidine-rich region. The olivine inclusion is also intruded by such a vein (Fig. 3c). Enrichment of the albite component (Table 9) is observed at the rounded end of such vein or nodule. This chemical zoning suggests intrusion of K-rich melt. Large crystal sizes and uniform chemical composition of the mafic silicates cannot be explained by growth from ordinary shock melt by a small-scale impact. They may be explained, in principle, by a shock melt that had few nucleation sites and cooled slowly, enriching K in the residual melt. The oval shaped olivine is in line with the proposal that olivine is a relict phase as in Miles (Ikeda et al., 1997a). The uniform REE distributions of the C1LF olivine (Fig. 9) also support this proposal. Parts of orthopyroxene (most likely dusty core) may also be of similar origin. However, the tiny euhedral inclusions of K-Na feldspar and chromite in orthopyroxene indicate that some of the orthopyroxene existed with a melt rich in K, Na, Cr, and Si. The textures of the K-feldspar-orthopyroxene vein in an olivine nodule in the surface inclusion suggest that the original mineralogy of olivine and pyroxene was modified by the K-, Si-rich melt intruded into the olivine crystal and reacted with olivine to produce orthopyroxene.

The presence of the K-rich melt is plausible from the textures of the sanidine veins, but the origin is not clear from known phase relations. The albitic glass compositions of the interior inclusions are distributed toward quartz in the quartz-(Ab + An)-Or system and not toward K-feldspar (Or) as differentiation proceeds (Fig. 7). The Na enrichment at the end of the K-feldspar nodule is not consistent with such trend. Therefore, K-rich compositions could not have been produced by differentiation of the sodic melt common in the interior inclusions. Nearly identical compositions of diopside and orthopyroxene between the Na-rich and K-rich inclusions, suggest that these minerals originated from similar (or the same) sources. Thus, the K-rich compositions may represent a separate melt. Another possibility is a fluid phase that leached K from surrounding materials and deposited it at the metal-silicate interface. The recent discovery of NaCl and KCl in the Monohans 1998 H5 chondrite (Zolensky et al., 1999) shows that K-rich liquids can exist on meteorite parent bodies. Then, either the precipitates (or perhaps the fluid itself) were incorporated into a silicate melt, producing the K-rich melt from which the surface inclusions formed. The coexisting Na- and K-feldspars in the E chondrites (Kimura and El Goresy, 1988) may have a similar origin.

Cooling of the surface inclusions was rapid enough to preserve the high sanadine structure in the C1LF inclusion (Wasserburg et al., 1968). Chemical zonings toward the albitic composition (Fig. 4a) at the rims of some parts of the sanidine crystals (Fig. 3) also suggest rapid cooling of the surface inclusion.

Up to this work, sanidine in Colomera has been interpreted as a product of extensive differentiation, when irons were separated from silicate melts. However, our observations do not support this idea. In this article, we propose that the K-rich melts were produced by inhomogeneous segregation as was proposed for the origin of Na-rich melt in the IAB irons (Takeda et al., 2000).

4.4. Comparisons with Other IIE and IAB Irons

The record of how the evolved silicate inclusions in Colomera were produced from the chondritic Netschaëvo-like inclusions is not preserved among differentiated IIE irons. It is our general understanding that there should be common basic processes for formation of certain mineral assemblage during the accretion and evolution of a planetesimal to make a meteorite parent body. Therefore, comparison of similar mineral assemblages found in different classes of meteorites or subclasses of irons give us information on a common formation process.

Silicate inclusions in the IIE irons, Netschaëvo and Watson, have affinities to recrystallized chondrites (e.g., Bild and Wasson, 1977). Y791093 (unique meteorite) consists of silicate inclusions texturally and mineralogically similar to recrystallized H chondrites and metal-sulfide-rich portions similar to primitive IIE irons (Ikeda et al., 1997b). Miles (IIE) contains inclusions ranging from gabbroic to cryptocrystalline (Ikeda and Prinz, 1996; Ikeda et al., 1997a). This mineral assemblage is similar to those found by us in the Colomera interior inclusions. Although eight IIE irons show us pictures of parts of the parent body, they are not enough to reconstruct the entire view. We therefore use the silicates in IAB irons to fill in the gaps in IIE history. In particular, to help make the case that feldspathic melts were produced by partial melting of ordinary-chondrite like materials, we discuss materials seen locally in the Caddo County IAB ion meteorite (Takeda et al., 2000). The similarity of ^{39}Ar-^{40}Ar degassing patterns of Colomera and Caddo County (Bogard et al., 2000) suggest at least parts of a thermal history of Colomera resemble that of Caddo County.

The IAB irons and winonaites have essentially identical oxygen isotope compositions and probably formed on the same parent body. The IAB irons also contain albite-diopside-rich (andesitic) material like that in IIE irons. In the IAB iron, Caddo County, a recrystallized chondritic region similar to the material in winonaites is located not far from metal-rich region with Na-Ca-Al-rich materials similar to those in Colomera. A funnel-like region extends from this recrystallized region to an albite-diopside-rich region, with an increasing abundance of elongated, larger plagioclase and diopside. This texture suggests that a partial melt segregated from the chondritic region and accumulated to form an albite-diopside-rich material. The similarity in the REE patterns of the albite-diopside-rich ma-

terial in Caddo County (Takeda et al., 2001, 2002) and of the Colomera bulk silicates (Hsu et al., 1997) also supports a similar origin of the partial melts on a much larger scale. The process responsible for phase segregation is called "Marangoni convection." The driving force is the difference in surface energy between the solids and melts involved. In Caddo County, the lengths of migration range from a few cm to more than 10 cm, but for Colomera inclusion the migration may have operated over a much longer distance. We suggest that in Colomera, as in the winonaites and Caddo County, a broadly chondritic source material was partially melted and the Na-Si-rich partial melt and Fe-Ni-S eutectic melt were separated from its source region. The mixing event that put molten metal in contact with silicate to make Colomera must have taken place before the partial melts completely crystallized.

4.5. Origin of Colomera and Other IIE Irons

The fundamental issues that relate to the formation of Colomera are: (1) the origin of masses of totally or partially molten FeNi metal; (2) the origin of the highly fractionated silicate melts that entered the molten metal and were entrapped; (3) the manner in which the metal and silicate melts were brought together in a regime permitting rapid crystallization of the metal and silicate; 4) rapid cooling at high temperature as shown by silicate textures and slow cooling at lower temperatures to produce Widmanstätten textures.

Molten metal may have been relatively common in the interior of asteroids in the early solar system. If ^{26}Al was present at an abundance of $^{26}Al/^{27}Al \sim 5\times10^{-6}$, then the interior of any body with a radius greater than ~30 km should have been heated to temperatures above the Fe-FeS eutectic, permitting the segregation of a molten metal core (Miyamoto and Takeda, 1994). Higher initial ratios would have produced melting in smaller bodies. At temperatures approaching 1100°C, low-temperature feldspathic silicate melts would also be produced. Observations from the winonaites suggest that silicate and metal melts may have coexisted in close proximity (Yugami et al., 1999; Takeda et al., 2000). However, in the case of Colomera, a simple model involving the mixing of two low-temperature melts in the interior of an asteroid is inconsistent with the rapid cooling of Colomera from high temperature.

Formation models of the IIE irons presented previously proposed an impact event or collision (Armstrong et al., 1990; Olsen et al., 1994; Ikeda and Prinz, 1996). Collisions involving 10-km-sized objects would have molten Fe-Ni masses available in the interiors that could be emplaced on or near planetary surfaces by the collision. Evidence for impacting molten metal (Hassanzadeh et al., 1990), is found in mesosiderites at somewhat younger times (cf. Stewart et al., 1996). One possibility is that the metal melt was sufficiently hot to generate a low-temperature silicate partial melt of surrounding chondritic material, although for this to occur the metal would have had to have been hotter than ~1400°C. Although a eutectic metal melt can exist at temperatures down to ~980°C, higher temperatures would be required to generate the low-temperature silicate partial melts. The common occurrence of Cr diopside and Na plagioclase in many globular inclusions (Table 1), their fairly constant compositions (Figs. 4, 5, and 9), and angular boundaries between Cr diopside and metal (Figs. 2a,c) indicate that these mineral crystals grew in the Na-Si-Al-Ca-Cr-rich melt before incorporation into the metal to form silicate inclusions. The molten metal may have been introduced into a region where large volumes of this crystal mush were already present, or may have coexisted with the crystal mush. Mixing of partly molten metal with the crystal mush could have induced additional melting in the silicates.

The Na-rich silicate melt probably formed via partial melting and segregation in a manner analogous to that which produced the melts in Caddo County (IAB) (Takeda et al., 2000). However, segregation of the Na-rich silicate melts was much more effective in the Colomera precursor than in Caddo County. The partial melts of the IAB irons accumulated within a few centimeters of the source region, whereas the crystal mush that became Colomera inclusions could have been meters across. After the silicate melt and Fe-Ni-S eutectic melt had segregated and the silicate melt had partially crystallized into crystal mush, a disturbance, most probably an impact, took place to mix these crystal mush and metal. In this scenario, we need not invoke the melting of the metal by an impact event. Partially molten metal somehow encapsulated "blobs" of silicate melt. Once a silicate melt was trapped in the metal, the each inclusion became, to first order, a closed system and evolved independently. The mixed metal and silicate cooled quickly in the high-temperature regime. This rapid cooling implies that the mixing of metal and silicate happened at a relatively shallow depth on the parent body. However, the final cooling through the lower temperature regime would have been much slower to permit development of the Widmanstätten structure.

Our model for Colomera has several features in common with the models of Ruzicka et al. (1999) for inclusions in IIE iron, Weekeroo Station, including evidence for remelting to produce glass, evidence for physical mixing of phases, evidence that at least some pyroxene grains in inclusions are relict or xenocrystic, and evidence for disequilibrium in the formation of glass. A major difference between our model and Ruzicka's concerns proposed impact or collision events. Ruzicka et al. (1999) and some other investigators emphasized that IIE iron meteorites could have formed by the collision between an FeNi-metal impactor and either a differentiated or undifferentiated silicate-rich target of H-chondrite affinity. Impact melting of metal and silicate is an explicit part of their scenarios. Our model proposes an impact to mix locally segregated partially molten FeNi-metal and the crystal mush. We do not exclude an impact to induce melting of chondritic materials, but Colomera did not keep the record of this event.

5. SUMMARY AND CONCLUSIONS

(1) There is a common occurrence of globular inclusions in Colomera with compositions that are very restricted and typified by a mineralogy of Na plagioclase and Cr diopside. There are many examples of spherical glassy inclusions enclosed in FeNi metal. These assemblages cannot be made by impact melting of the H chondrites. (2) Some crystallization of silicates occurred before incorporation into the FeNi melt. (3) Silicate crystal mush was enclosed in partly liquid FeNi metal. Different proportions of crystals and melt were acquired by each inclusion. Additional crystallization occurred in the

trapped silicate melts. (4) The whole assemblage cooled rapidly enough to quench the high viscosity silicate melts and to preserve high-sanidine. (5) The final cooling of Colomera in the temperature regime of 600°C and below was slow enough to develop Widmanstätten structure. (6) The K-rich surface inclusion provides strong evidence for the presence of a K-Si-rich melt. Such a melt is difficult to explain by the differentiation of Na-Ca-rich melt. (7) The K-rich material may have originated as a fluid phase that leached K from surrounding materials and segregated by a mechanism similar to that proposed for the Na-rich inclusions.

Acknowledgments—This work was supported by a Grant-in-Aid for Science Research from the Japanese Ministry of Education, Science and Culture and by a grant from the Ocean Research Institute, University of Tokyo, and is carried out as a part of Ground Research Announcement for Space Utilization, promoted by the Japan Space Forum. Additional support came from NASA grants NAG5-4083 to G. J. Wasserburg and NAG-58158 to G.R.H. We thank G. J. Wasserburg for providing samples for this work, for use of his laboratory facilities, for helpful discussions, and for inviting the senior author to Caltech for an extended stay. We acknowledge Lindsey Hedges, P. Carpenter and R. Osada, M. Otsuki, Drs. T. Ishii, K. Yugami, J. Chikami, and Don Bogard for their help in microanalysis and sample preparations. We are indebted to Y. Ikeda, P. Wyllie, M. Miyamoto, P. Warren, K. Keil, Y. Kato, and Drs. M. Kimura, H. Ohashi, and T. Mikouchi for discussion and to Drs. John Longhi and K. Saiki and H. Ogata for preparing the relevant diagrams. Careful reviews and constructive comments by Drs. Alex Ruzicka and H. Palme and anonymous reviewers substantively improved this article. Caltech Division Contribution 8733(1064).

Associate editor: H. Palme

REFERENCES

Armstrong J. T., Kennedy A. K., Carpenter P. K., and Albee A. L. (1990) Petrography and trace element chemistry of Colomera (IIE) silicate inclusions: Rhyolitic plums in the pudding. *Lunar Planet. Sci.* **21,** 22–23.

Bence A. E. and Burnett D. S. (1969) Chemistry and mineralogy of the silicates and metal of the Kodaikanal meteorite. *Geochim. Cosmochim. Acta* **33,** 387–407.

Bild R. W. and Wasson J. T. (1977) Netschaëvo: A new class of chondritic meteorite. *Science* **197,** 58–62.

Bogard D. D., Burnett D. S., and Wasserburg G. J. (1969) Cosmogenic rare gases and the ^{40}Ar-^{39}Ar age of the Kodaikanal iron meteorite. *Earth Planet. Sci. Lett.* **5,** 273–281.

Bogard D. D., Garrison D. H., and McCoy T. J. (2000) Chronology and petrology of silicates from IIE iron meteorites: Evidence of a complex parent body evolution. *Geochim. Cosmochim. Acta* **64,** 2133–2154.

Bunch T. E. and Olsen E. (1968) Potassium feldspar in Weekeroo Station, Kodaikanal, and Colomera iron meteorites. *Science* **160,** 1223–1225.

Bunch T. E., Keil K., and Olsen E. (1970) Mineralogy and petrology of silicate inclusions in iron meteorites. *Contr. Mineral. Petrol.* **25,** 297–340.

Burnett D. S. and Wasserburg G. J. (1967) ^{87}Rb-^{87}Sr ages of silicate inclusions in iron meteorites. *Earth Planet. Sci. Lett.* **2,** 397–408.

Casanova I., Graft T., and Marti K. (1995) Discovery of an unmelted H-chondrite inclusion in an iron meteorite. *Science* **268,** 469–608.

Clayton R. N., Mayeda T. K., Olsen E. J., and Prinz M. (1983) Oxygen isotope relationships in iron meteorites. *Earth Planet. Sci. Lett.* **65,** 229–232.

Fahey A. J., Goswami J. N., McKeegan K. D., and Zinner E. (1987) ^{26}Al, ^{244}Pu: ^{50}Ti, REE and trace element abundances in hibonite grains from CM and CV meteorites. *Geochim. Cosmochim. Acta* **51,** 329–350.

Floss C. (2000) Complexities on the acapulcoite-lodranite parent body: Evidence from trace element distributions in silicate minerals. *Geochim. Cosmochim. Acta* **35,** 1073–1085.

Hassanzadeh J., Rubin A. E., and Wasson J. T. (1990) Compositions of large metal nodules in mesosiderites: Links to iron meteorite group IIIAB and the origin of mesosiderite subgroups. *Geochim. Cosmochim. Acta* **54,** 3197–3208.

Hsu W., Takeda H., Huss G. R., and Wasserburg G. J. (1997) Mineralogy and chemistry of Colomera (IIE) silicate inclusions. *Meteor. Planet. Sci.* **32,** A61–62.

Ikeda Y. and Prinz M. (1996) Petrology of silicate inclusions in the Miles IIE iron. *Proc. NIPR Symp. Antarct. Meteorites* **9,** 143–173.

Ikeda Y., Yamamoto T., Kojima H., Imae N., Kong P., Ebihara M., and Prinz M. (1997a) Yamato-791093, a metal-sulfide–enriched H-group chondritic meteorite transitional to primitive IIE irons with silicate inclusions. *Antarct. Meteorite Res.* **10,** 335–353.

Ikeda Y., Ebihara M., and Prinz M. (1997b) Petrology and chemistry of the Miles IIE iron. I: Description and petrology of twenty new silicate inclusions. *Antarct. Meteorite Res.* **10,** 355–372.

Kimura M. and El Goresy A. (1988) Djerfisherhite compositions in EH chondrites: A potential parameter to the geochemistry of the alkali elements. *Meteoritics* **23,** 279–280.

Longhi J. (1991) Comparative liquids equilibria of hypersthene-normative basalts at low pressure. *Am. Mineral.* **76,** 785–800.

McCoy T. J. (1995) Silicate-bearing IIE irons: Early mixing and differentiation in a core-mantle environment and shock resetting of ages. *Meteoritics* **30,** 542–543.

McCoy T. J., Keil K., Muenow D. W., and Wilson L. (1997) Partial melting and melt migration in the acapulcoite-lodranite parent body. *Geochim. Cosmochim. Acta* **61,** 639–650.

Miyamoto M. and Takeda H. (1994) Thermal history of lodranites Yamato 74357 and MAC88177 as inferred from the chemical zoning of pyroxene and olivine. *J. Geophys. Res.* **99,** 5669–5677.

Ohashi H. and Fujita T. (1979) Crystal chemistry of kosmochlor-diopside solid solutions. *J. Jpn. Assoc. Min. Petrol. Econ. Geol.* **74,** 16–26.

Ohashi H., Fujita T., and Osawa T. (1982) The crystal structure of $NaTiSi_2O_6$ pyroxene. *J. Jpn. Assoc. Min. Petrol. Econ. Geol.* **77,** 305–309.

Olsen E., Davis A., Clarke R. S. Jr., Schultz L., Weber H. W., Clayton R., Mayeda T., Jarosewich E., Sylvester P., Grossman L., Wang M.-S., Lipschutz M. E., Steele I. M., and Schwade L. (1994) Watson: A new link in the IIE iron chain. *Meteoritics* **29,** 200–213.

Osadchii Eu. G., Baryshnikova G. V., and Novikov G. V. (1981) The Elga Meteorite: Silicate inclusions and shock metamorphism. *Proc. Lunar Planet. Sci. Conf.* **12B,** 1049–1068.

Prinz M., Nehru C. E., Delaney J. S., Weisberg M., and Olsen E. (1983) Globular silicate inclusions in IIE irons and Sombrerete: Highly fractionated minimum melts. *Lunar Planet. Sci.* **14,** 618–619.

Ruzicka A., Fowler G. W., Snyder G. A., Prinz M., Papike J. J., and Taylor L. A. (1999) Petrogenesis of silicate inclusions in the Weekeroo Station IIE iron meteorite: Differentiation, remelting, and dynamic mixing. *Geochim. Cosmochim. Acta* **63,** 2123–2143.

Sakamoto S. and Takasu A. (1996) Kosmochlor from the Osayama ultramafic body in the Sangun metamorphic belt, southwest Japan. *J. Geol. Soc. Jpn.* **102,** 49–52.

Sanz H. G., Burnett D. S., and Wasserburg G. J. (1970) A precise ^{87}Rb-^{87}Sr ages and initial ^{87}Sr-^{86}Sr for the Colomera iron meteorite. *Geochim. Cosmochim. Acta* **34,** 1227–1239.

Schairer J. F. and Yoder H. S. Jr (1960) The nature of residual liquid from crystallization, with data on the system nepheline-diopside-silica. *Am. J. Sci.* **258A,** 278.

Scott E. R. D. and Wasson J. T. (1976) Chemical classification of iron meteorites—VIII. Groups IC, IIE, IIIF and 97 other irons. *Geochim. Cosmochim. Acta* **40,** 103–115.

Stewart T. D., Papanastassiou D. A., and Wasserburg G. J. (1996) Sm-Nd systematics of a silicate inclusion in the Caddo IAB iron meteorite. *Earth Planet. Sci. Lett.* **143,** 1–12.

Takeda H. (1997) Mineralogical records of early planetary processes on the howardite, eucrite, diogenite parent body with reference to Vesta. *Meteor. Planet. Sci.* **32,** 841–853.

Takeda H., Baba T., Saiki K., Otsuki M., and Ebihara M. (1993) A plagioclase-augite inclusion in Caddo County: Low-temperature melt of primitive achondrites (abstract). *Meteoritics* **28,** 447.

Takeda H., Mori H., Hiroi T., and Saito J. (1994) Mineralogy of new Antarctic achondrites with affinity to Lodran and a model of their evolution in an asteroid. *Meteoritics* **29,** 830–842.

Takeda H., Yugami K., Bogard D., and Miyamoto M. (1997) Plagioclase-augite-rich gabbro in the Caddo County IAB iron, and the missing basalts associated with iron meteorites. *Lunar Planet. Sci.* **28,** 1409–1410.

Takeda H., Bogard D. D., Mittlefehldt D. W., and Garrison D. H. (2000) Mineralogy, petrology, chemistry, and ^{39}Ar-^{40}Ar and exposure ages of the Caddo County IAB iron: Evidence for early partial melt segregation of a gabbro area rich in plagioclase-diopside. *Geochim. Cosmochim. Acta* **64,** 1311–1327.

Takeda H., Hsu W., and Ogata H. (2001) Trace element chemistry of minerals in chemically andesitic material in the Caddo County IAB iron meteorite. *Antarctic Meteorites* **26,** 135–137.

Takeda H., Hsu W., and Ogata H. (2002) Mineralogy and trace element chemistry of plagioclase and Ca phosphate in some Antarctic lodranites. *Antarctic Meteorites* **27,** 157–159.

Wasserburg G. J., Sanz H. G., and Bence A. E. (1968) Potassium feldspar phenocrysts in the surface of Colomera, an iron meteorite. *Science* **161,** 684–687.

Wasson J. T., Ouyang X., and Jerde E. (1989) Chemical classification of iron meteorites XI: Multi-element studies of 38 new irons and the high abundance of ungrouped irons from Antarctica. *Geochim. Cosmochim. Acta* **53,** 735–744.

Yugami K., Takeda H., Kojima H., and Miyamoto M. (1998) Modal mineral abundances and the differentiation trends in primitive achondrites. *Antarct. Meteorite Res.* **11,** 49–70.

Yugami K., Takeda H., Kojima H., and Miyamoto M. (1999) Comparisons of textural and chemical variations of minerals in some primitive achondrites and an H7 chondrite, with reference to their formation and cooling histories. *Antarct. Meteorite Res.* **12,** 117–138.

Zinner E. and Crozaz G. (1986) A method for the quantitative measurement of rare earth elements in the ion microprobe. *Int. J. Mass Spectrom. Ion Processes* **69,** 17–38.

Zolensky M. E., Bodnar R. J., Bogard D. D., Garrison D. H., Gibson E. K., Nyquist L. E., Reese Y., Shih C.-Y., and Weismann H. (1999) The first direct samples of asteroidal water: Fluid inclusion–bearing halite in an H5 chondrite. *Science* **285,** 1377–1379.